Synthesis, Structure, and Protonation Studies of $Cp^*MH_3(dppe)$ (M = Mo, W). Pseudo-Trigonal-Prismatic vs Pseudo-Octahedral Structures for Half-Sandwich Group 6 M(IV) Derivatives

Brett Pleune,[1a] Rinaldo Poli,*[,1b] and James C. Fettinger[1a]

Department of Chemistry and Biochemistry, University of Maryland, College Park, Maryland 20742, and Laboratoire de Synthèse et d'Electrosynthèse Organométallique, Faculté des Sciences "Gabriel", Université de Bourgogne, 6 Boulevard Gabriel, 21100 Dijon, France

Received November 27, 1996[⊗]

The compounds $Cp^*MH_3(dppe)$ (M = Mo, **1**; W, **2**) are accessible in good yields from reacting the corresponding compound Cp^*MCl_4 and $LiAlH_4$ in toluene/Et_2O followed by methanolysis. The X-ray structure of **1** shows a pseudo-trigonal-prismatic geometry which is unprecedented for half-sandwich $CpML_5$-type compounds. Protonation with $HBF_4{\cdot}Et_2O$ in Et_2O at low temperature affords $[Cp^*MH_4(dppe)]^+BF_4^-$ salts (M = Mo, **3**; W, **4**). While **3** spontaneously decomposes, even at low temperatures, in coordinating solvents and CH_2Cl_2, **4** is stable at room temperature in MeCN. An X-ray structure of **4** is consistent with a classical tetrahydrido species with a distorted pseudo-pentagonal-bipyramidal structure. The low-temperature NMR properties, $J_{HD} \leq 1$ Hz for **4**-d_3, and the $T_{1(min)}$ value for the hydride resonance are also consistent with this structural assignment. Decomposition of **3** in MeCN at room temperature selectively affords $[Cp^*MoH_2(MeCN)(dppe)]^+BF_4^-$, **5**. The NMR properties of this complex indicate a fluxional structure with inequivalent H and P nuclei and are consistent with a pseudo-trigonal-prismatic structure analogous to that of the precursor **1**. Further protonation of **5** in MeCN or direct protonation of **1** with excess acid in MeCN affords two isomers of complex $[Cp^*MoH(MeCN)_2(dppe)](BF_4)_2$, **6** and **7**. Thermal treatment in MeCN slowly converts **7** into **6** initially, but both isomers further transform into a third isomer, **8**, upon prolonged heating. The structure of **6** has been elucidated by X-ray crystallography and consists of a highly distorted pseudo-octahedral geometry with relative *trans* MeCN ligands. The structures of **7** and **8** and mechanisms of the interconversions between the various isomeric structures are proposed on the basis of the solution NMR studies.

Introduction

Transition metal polyhydride systems have been the focus of much recent attention. The dichotomy between classical and nonclassical hydrides[2−4] and possible mechanisms of hydride fluxionality[5] have been studied extensively. A few mononuclear transient 17-electron polyhydride species have been produced by either chemical or electrochemical oxidation of the saturated polyhydride precursors,[6−16] whereas a greater body of work has been carried out on monohydride systems.[17−40] The transient 17-electron species, $[M-H]^{+\bullet}$, usually decomposes by deprotonation,[24] the outcome being

[⊗] Abstract published in *Advance ACS Abstracts,* March 15, 1997.

(1) (a) University of Maryland. (b) Université de Bourgogne.
(2) Hamilton, D. G.; Crabtree, R. H. *J. Am. Chem. Soc.* **1988**, *110*, 4126−4133.
(3) Luo, X.-L.; Crabtree, R. H. *Inorg. Chem.* **1990**, *29*, 2788−2791.
(4) Van Der Sluys, L. S.; Eckert, J.; Eisenstein, O.; Hall, J. H.; Huffman, J. C.; Jackson, S. A.; Koetzle, T. F.; Kubas, G. J.; Vergamini, P. J.; Caulton, K. G. *J. Am. Chem. Soc.* **1990**, *112*, 4831−4841.
(5) Gusev, D. G.; Berke, H. *Chem. Ber.* **1996**, *129*, 1143−1155 and references therein.
(6) Klinger, R. J.; Huffman, J. C.; Kochi, J. K. *J. Am. Chem. Soc.* **1980**, *102*, 208−216.
(7) Allison, J. D.; Cameron, C. J.; Wild, R. E.; Walton, R. A. *J. Organomet. Chem.* **1981**, *218*, C62−C66.
(8) Rhodes, L. F.; Zubkowski, J. D.; Folting, K.; Huffman, J. C.; Caulton, K. G. *Inorg. Chem.* **1982**, *21*, 4185−4192.
(9) Bruno, J. W.; Caulton, K. G. *J. Organometal. Chem.* **1986**, *315*, C13−C16.
(10) Detty, M. R.; Jones, W. D. *J. Am. Chem. Soc.* **1987**, *109*, 5666−5673.
(11) Costello, M. T.; Walton, R. A. *Inorg. Chem.* **1988**, *27*, 2563−2564.
(12) Herrmann, W. A.; Theiler, H. G.; Herdtweck, E.; Kiprof, P. *J. Organometal. Chem.* **1989**, *367*, 291−311.
(13) Bianchini, C.; Laschi, F.; Peruzzini, M.; Ottaviani, F.; Vacca, A.; Zanello, P. *Inorg. Chem.* **1990**, *29*, 3394−3402.
(14) Roullier, L.; Lucas, D.; Mugnier, Y.; Antiñolo, A.; Fajardo, M.; Otero, A. *J. Organometal. Chem.* **1991**, *412*, 353−362.
(15) Westerberg, D. E.; Rhodes, L. F.; Edwin, J.; Geiger, W. E.; Caulton, K. G. *Inorg. Chem.* **1991**, *30*, 1107−1112.
(16) Zlota, A. A.; Tilset, M.; Caulton, K. G. *Inorg. Chem.* **1993**, *32*, 3816−3821.
(17) Sanders, J. R. *J. Chem. Soc., Dalton Trans.* **1973**, 748−749.
(18) Sanders, J. R. *J. Chem. Soc., Dalton Trans.* **1975**, 2340−2342.
(19) Gargano, M.; Giannoccaro, P.; Rossi, M.; Vasapollo, G.; Sacco, A. *J. Chem. Soc., Dalton Trans.* **1975**, 9−12.
(20) Pilloni, G.; Schiavon, G.; Zotti, G.; Zecchin, S. *J. Organometal. Chem.* **1977**, *134*, 305−318.
(21) Treichel, P. M.; Molzahn, D. C.; Wagner, K. P. *J. Organometal. Chem.* **1979**, *174*, 191−197.
(22) Chen, L.; Davies, J. A. *Inorg. Chim. Acta* **1990**, *175*, 41−45.
(23) Roullier, L.; Lucas, D.; Mugnier, Y.; Antiñolo, A.; Fajardo, M.; Otero, A. *J. Organometal. Chem.* **1990**, *396*, C12−C16.
(24) Ryan, O. B.; Tilset, M.; Parker, V. D. *J. Am. Chem. Soc.* **1990**, *112*, 2618−2626.
(25) Ryan, O. B.; Smith, K.-T.; Tilset, M. *J. Organometal. Chem.* **1991**, *421*, 315−322.
(26) Ryan, O. B.; Tilset, M.; Parker, V. D. *Organometallics* **1991**, *10*, 298−304.
(27) Ryan, O. B.; Tilset, M. *J. Am. Chem. Soc.* **1991**, *113*, 9554−9561.

S0276-7333(96)01002-3 CCC: $14.00

determined by the basic properties of the solvent vs M−H as well as by the reactivity of the depronotated product M•. In particular, when the starting compound M−H captures the proton, the resulting $[MH_2]^+$ species may either remain as a stable (classical or nonclassical) hydride product or lead to the replacement of one or more H_2 molecules with as many molecules of a monodentate ligand (usually a coordinative solvent). A study of the protonation of transition metal hydrides, therefore, gives useful information on the possible nature of the ultimate oxidation products. In a recent study of the oxidation and protonation of the monohydride system $CpMoH(CO)_2(PR_3)$ (R = Me, Ph) in acetonitrile,[41] we have shown that proton transfer from the 17-electron $[CpMoH(CO)_2(PR_3)]^{+\bullet}$ transient to the starting unoxidized hydride or the direct protonation of the latter by HBF_4 is followed by an irreversible H_2 loss, which drives either reaction to the selective formation of the solvato complex $[CpMo(MeCN)(CO)_2(PR_3)]^+$. Polyhydrides show the same general reactivity patterns as monohydrides; for instance, treatment of $Cp^*Ru(PPh_3)H_3$ with $Cp_2Fe^+PF_6^-$ in MeCN leads to H_2 evolution and formation of $[Cp^*Ru(PPh_3)(MeCN)_2]^+$.[15]

With the ultimate goal in mind of generating stable 17-electron polyhydride species for further activation and reactivity studies, we have synthesized new compounds of the general class (η^5-ring)MH_3L_2 (ring = cyclopentadienyl ligand, M = group 6 metal, L = tertiary phosphine), previously reported examples of which include $CpMoH_3(dppe)$,[42] $CpWH_3(PMe_3)_2$,[43] (η^5-$C_5H_4Pr^i$)MoH_3L_2 (L = PMe_3, PMe_2Ph or L_2 = dppe),[44] $Cp^*MoH_3(PMe_3)_2$,[45] and $CpMoH_3(PMe_2Ph)_2$.[46] Oxidation studies of these derivatives had not previously been reported, while protonation studies were limited to (η^5-$C_5H_4Pr^i$)$MoH_3(PMe_3)_2$ with HCl and water to generate $[(\eta^5\text{-}C_5H_4Pr^i)MoO(PMe_3)_2]^+$.[44] In this contribution, we will examine the protonation of the new polyhydride species $Cp^*MH_3(dppe)$ (M = Mo, **1**; W, **2**). Oxidation studies of these compounds will be documented in a later contribution. Part of these studies have been previously communicated.[47]

Experimental Section

All manipulations were carried out under an inert atmosphere of dinitrogen or argon by the use of Schlenk-line or glovebox techniques. Methanol was degassed by three freeze−pump−thaw cycles prior to use. Other solvents were dried by conventional methods (Et_2O from Na/K/benzophenone, toluene and heptane from Na, MeCN from CaH_2, and CH_2Cl_2 from P_4O_{10}) and distilled under dinitrogen prior to use. Deuterated solvents were dried over molecular sieves and degassed by three freeze−pump−thaw cycles prior to use. ^{1}H- and ^{31}P{^{1}H}-NMR measurements were carried out on Bruker AF200, WP200, or AM400 spectrometers; the peak positions are reported with positive shifts downfield of TMS, as calculated from the residual solvent peaks (^{1}H), or downfield of external 85% H_3PO_4 (^{31}P). For each ^{31}P-NMR spectrum, a sealed capillary containing 85% H_3PO_4 was immersed in the same NMR solvent used for the measurement and this was used as the reference. ^{31}P{selective-^{1}H}-NMR measurements were carried out on Bruker WP200 or AM400 spectrometers. ^{1}H{^{31}P}-NMR measurements were carried out on a Bruker AMX500 spectrometer. Values of the longitudinal relaxation times T_1 were obtained from the slopes of linear plots of ln $[2I_{eq}/(I_{eq} - I_\tau)]$ vs τ, where I_τ is the peak intensity as measured by the standard inversion−recovery−pulse (180−τ−90) sequence and I_{eq} is the peak intensity at $\tau = \infty$. EPR measurements were carried out at the X band microwave frequency on a Bruker ER 200 D spectrometer upgraded to ESP 300, equipped with a cylindrical ER/4103 TM 110 cavity. The elemental analyses were carried out by Desert Analytics, Tucson, AZ, and by Atlantic Microlab, Norcross, GA. $LiAlH_4$, dppe, grade I acidic alumina, and HBF_4·Et_2O (Aldrich) were used without further purification. $CDFCl_2$,[48] Cp^*MoCl_4,[49] and Cp^*WCl_4[50] were prepared according to literature procedures.

Synthesis of $Cp^*MoH_3(dppe)$ (1). Cp^*MoCl_4 (1.007 g, 2.70 mmol) was slurried in a 70 mL:15 mL toluene/diethyl ether solvent mixture at room temperature. The ligand dppe (1.074 g, 2.70 mmol) and $LiAlH_4$ (1.00 g, 26.3 mmol) were added to the stirring solution at room temperature. The mixture began to slowly evolve H_2 gas as the solution developed an orange color within 30 min. The mixture was stirred for an additional 12 h at room temperature. Dropwise addition of MeOH (ca. 10 mL) at room temperature caused vigorous evolution of H_2 gas; the orange solution darkened. The reaction mixture was stirred an additional 30 min, followed by evaporation of the mixture to dryness. The residue was extracted with heptane (150 mL) and filtered through Celite. The resulting yellow-orange solution was evaporated to ca. 2 mL, precipitating a yellow powder, which was washed with with cold (−80 °C) heptane and dried under vacuum. Yield: 1.107 g (65%). Single crystals were obtained from a saturated warm heptane solution upon cooling to room temperature. Anal. Calcd for $C_{36}H_{42}MoP_2$: C, 68.4; H, 6.7. Found: C, 67.6; H, 7.0. ^{1}H-NMR (C_6D_6, δ): 7.8−7.0 (m, 20H, dppe−Ph), 1.85 (m, 4H, dppe−CH_2), 1.83 (s, 15H, Cp*), −5.27 (t, J_{PH} = 42.0 Hz, 3H, MoH). ^{31}P-NMR (C_6D_6, δ): 91.8 (s). ^{31}P{selective-^{1}H}-NMR (C_6D_6, δ): 91.8 (quartet, J_{PH} = 41.0 Hz).

Synthesis of $Cp^*WH_3(dppe)$ (2). Cp^*WCl_4 (1.46 g, 3.17 mmol) was slurried in a 100 mL:15 mL toluene/diethyl ether solvent mixture at room temperature. The ligand dppe (1.26 g, 3.17 mmol) and $LiAlH_4$ (1.20 g, 31.6 mmol) were added to

(28) Roger, C.; Hamon, P.; Toupet, L.; Rabaâ, H.; Saillard, J.-Y.; Hamon, J.-R.; Lapinte, C. *Organometallics* **1991**, *10*, 1045−1054.
(29) Hamon, P.; Toupet, L.; Hamon, J.-R.; Lapinte, C. *Organometallics* **1992**, *11*, 1429−1431.
(30) Tilset, M. *J. Am. Chem. Soc.* **1992**, *114*, 2740−2741.
(31) Jia, G.; Lough, A. J.; Morris, R. H. *Organometallics* **1992**, *11*, 161−171.
(32) Smith, K.-T.; Tilset, M. *J. Organometal. Chem.* **1992**, *431*, 55−64.
(33) Amatore, C.; Fraústo da Silva, J. J. R.; Guedes da Silva, M. F. C.; Pombeiro, A. J. L.; Verpeaux, J.-N. *J. Chem. Soc., Chem. Commun.* **1992**, 1289−1291.
(34) Skagestad, V.; Tilset, M. *J. Am. Chem. Soc.* **1993**, *115*, 5077−5083.
(35) Smith, K.-T.; Rømming, C.; Tilset, M. *J. Am. Chem. Soc.* **1993**, *115*, 8681−8689.
(36) Jiménez-Tenorio, M.; Puerta, M. C.; Valerga, P. *Organometallics* **1994**, *13*, 3330−3337.
(37) Kaim, W.; Reinhardt, R.; Sieger, M. *Inorg. Chem.* **1994**, *33*, 4453−4459.
(38) Pedersen, A.; Tilset, M. *Organometallics* **1994**, *13*, 4887−4894.
(39) Blaine, C. A.; Ellis, J. E.; Mann, K. R. *Inorg. Chem.* **1995**, *34*, 1552−1561.
(40) Hembre, R. T.; McQueen, J. S.; Day, V. W. *J. Am. Chem. Soc.* **1996**, *118*, 798−803.
(41) Quadrelli, E. A.; Kraatz, H.-B.; Poli, R. *Inorg. Chem.* **1996**, *35*, 5154−5162.
(42) Aviles, T.; Green, M. L. H.; Dias, A. R.; Romao, C. *J. Chem. Soc., Dalton Trans.* **1979**, 1367−1371.
(43) Green, M. L. H.; Parkin, G. *J. Chem. Soc., Dalton Trans.* **1987**, 1611−1618.
(44) Grebenik, P. D.; Green, M. L. H.; Izquierdo, A.; Mtetwa, V. S. B.; Prout, K. *J. Chem. Soc., Dalton Trans.* **1987**, 9−19.
(45) Abugideiri, F.; Kelland, M. A.; Poli, R.; Rheingold, A. L. *Organometallics* **1992**, *11*, 1303−1311.
(46) Abugideiri, F.; Fettinger, J. C.; Pleune, B.; Poli, R.; Bayse, C. A.; Hall, M. B. *Organometallics* **1997**, *16*, 1179−1185.
(47) Fettinger, J. C.; Pleune, B.; Poli, R. *J. Am. Chem. Soc.* **1996**, *118*, 4906−4907.
(48) Siegel, S. S.; Anet, F. A. *J. Org. Chem.* **1988**, *53*, 2629−2630.
(49) Keogh, D. W.; Poli, R. In *New Synthetic Methods of Organometallic and Inorganic Chemistry*; Herrmann, W. A., Ed.; Georg Thieme Verlag: Stuttgart, Germany.
(50) Murray, R. C.; Blum, L.; Liu, A. H.; Schrock, R. R. *Organometallics* **1985**, *4*, 953−954.

the stirring solution at room temperature. Slow evolution of H_2 gas was witnessed, as the solution developed an orange color within 30 min. The reaction mixture was stirred an additional 12 h, and the solvent was evaporated to dryness under vacuum. The residue was extracted into heptane (200 mL), and the solution was filtered through Celite. The orange solution was evaporated to ca. 2 mL, precipitating a crystalline orange powder. The powder was washed with with cold (−80 °C) heptane and dried under vacuum. Yield: 712 mg (32%). Heptane (50 mL) was added to the remaining residue, and 10 mL of methanol was added dropwise at room temperature. H_2 gas vigorously evolved, and the solution developed a red-orange color. The reaction mixture stirred for an additional 30 min and was filtered through Celite. The solution was evaporated to ca. 5 mL, precipitating a second crop of orange powder (498 mg). Combined yield: 1.21 g (53%). The second crop is slightly contaminated by the pentahydride compound Cp*WH$_5$(η^1-dppe) (see Results). Spectroscopically pure product is obtained from this crop by recrystallization from hot heptane. Anal. Calcd for $C_{36}H_{42}WP_2$: C, 60.0; H, 5.9. Found: C, 60.6; H, 5.9. ^{1}H-NMR (C_6D_6, δ): 7.8−7.0 (m, 20H, dppe−Ph), 2.1−1.9 (m, 4H, dppe−CH_2), 1.93 (s, 15H, Cp*), −5.90 (t, 3H, WH, J_{PH} = 44.6 Hz, J_{WH} = 54.4 Hz). ^{31}P-NMR (C_6D_6, δ): 67.9 (s, J_{WP} = 134.4 Hz). ^{31}P{selective-^{1}H}-NMR (C_6D_6, δ): 67.9 (quartet, J_{PH} = 41.5 Hz).

Synthesis of [Cp*MoH$_4$(dppe)]BF$_4$ (3). Cp*MoH$_3$(dppe) (836 mg, 1.30 mmol) was dissolved in 40 mL of diethyl ether. HBF$_4$·Et$_2$O (185 μL, 1.48 mmol) was added to the solution via microsyringe at room temperature. An off-white precipitate immediately developed. The supernatant liquid was removed by filter−cannula, and the product was washed with diethyl ether (3 × 10 mL) and dried under vacuum. Yield: 845 mg (90%). Anal. Calcd for $C_{36}H_{43}BF_4MoP_2$: C, 60.02; H, 6.02. Found: C, 58.18: H, 5.09. ^{1}H-NMR (CDFCl$_2$, −60 °C, δ): 7.9−7.0 (m, 20H, dppe−Ph), 2.25−2.20 (m, 4H, dppe−CH_2), 1.93 (s, 15H, Cp*), −3.56 (t, 4H, M−H, J_{PH} = 36.0 Hz). ^{31}P-NMR (CDFCl$_2$, −60 °C, δ): 72.9 (s). ^{31}P{selective-^{1}H}-NMR (CDFCl$_2$, −60 °C, δ): 72.9 (quintet, J_{PH} = 34.0 Hz). A better elemental analysis could not be obtained because of the decomposition of the compound upon attempted recrystallization (see Results).

Synthesis of [Cp*WH$_4$(dppe)]BF$_4$ (4). Cp*WH$_3$(dppe) (102 mg, 0.142 mmol) was dissolved in 10 mL of diethyl ether. HBF$_4$·Et$_2$O (20 μL, 0.16 mmol) was added to the solution via microsyringe at room temperature. An off-white precipitate immediately developed. The ether solvent was removed by filter−cannula, and the product was washed with diethyl ether (3 × 5 mL) and dried under vacuum. Yield: 99 mg (86%). Single crystals were grown from slow diffusion of a layer of diethyl ether into a saturated solution in CH_3CN at room temperature. Anal. Calcd for $C_{36}H_{43}BF_4P_2W$: C, 53.49; H, 5.36. Found: C, 53.03; H, 5.40. ^{1}H-NMR (CD_2Cl_2, δ): 7.8−7.3 (m, 20H, dppe−Ph), 2.4−2.0 (m, 4H, dppe−CH_2), 2.05 (s, 15H, Cp*), −2.73 (t, 4H, M−H, J_{PH} = 32.6 Hz, J_{WH} = 37.7 Hz). ^{31}P-NMR (CD_2Cl_2, room t, δ): 51.6 (s, J_{WP} = 126.6 Hz). ^{31}P{selec-^{1}H}-NMR (CD_2Cl_2, δ): 51.6 (quintet, J_{PH} = 28.4 Hz). ^{31}P-NMR (CDFCl$_2$, −95 °C, δ): 48.6 (d, J_{PP} = 26.3 Hz, J_{PW} = 139.5 Hz), 54.7 (d, J_{PP} = 26.3 Hz, J_{PW} = 139.5 Hz).

Synthesis of [Cp*MoH$_2$(dppe)(MeCN)]BF$_4$ (5). Compound **3** (110 mg, 0.153 mmol) was dissolved in 2 mL of CH_3CN at room temperature. The solution was stirred for 30 min; 10 mL of Et_2O was added to precipitate the product. The solution was filtered, and the yellow-brown residue was washed with Et_2O (3 × 5 mL). The product was dried under vacuum. Yield: 95 mg (82%). Anal. Calcd for $C_{38}H_{44}MoP_2NBF_4$·H_2O: C, 58.70; H, 5.96. Found: C, 58.2; H, 5.8. ^{1}H-NMR (CD_3CN, δ): 7.8−7.0 (m, 20H, dppe−Ph), 3.0−2.5 (m, 4H, dppe−CH_2), 1.99 (s, 3H, CH_3CN), 1.69 (s, 15H, Cp*), −5.50 (dd, 2H, M−H, $J_{P'H}$ = 51 Hz, $J_{P''H}$ = 52 Hz). A broad resonance at δ 2.2 (br), assigned to H_2O, is also observed. Upon broad-band ^{31}P decoupling, the ^{1}H-NMR resonance at δ −5.50 collapsed into a singlet. ^{31}P{^{1}H}-NMR (CD_3CN, δ): 78.1 (s). ^{31}P{selective-^{1}H}-NMR (CD_3CN, δ): 78.1 (t, J_{PH} = 52 Hz). ^{31}P{^{1}H}-NMR (CD_2Cl_2, −80 °C, δ): 82.8 (d, J_{PP} = 20.8 Hz), 75.3 (d, J_{PP} = 20.7 Hz).

Protonation of Cp*MoH$_3$(dppe) in Acetonitrile. HBF$_4$·Et$_2$O (7 μL, 0.040 mmol) was added to a suspension of Cp*MoH$_3$(dppe) (25 mg, 0.039 mmol) in 0.5 mL CD_3CN via microsyringe at room temperature. The insoluble yellow starting compound began to dissolve as the solution visibly evolved H_2, turning the solution from yellow-orange to red over a period of 60 min. The solution was monitored via ^{1}H- and ^{31}P-NMR spectroscopies showing a mixture of **5** and two isomers of compound [Cp*MoH(dppe)(MeCN)$_2$](BF$_4$)$_2$ (**6** and **7**). According to the Cp* resonances in the ^{1}H-NMR spectrum, compounds **5**, **6**, and **7** were approximately in a 6:1:3 ratio.

Synthesis of *trans*-[Cp*MoH(dppe)(MeCN)$_2$](BF$_4$)$_2$ (6). HBF$_4$·Et$_2$O (15 μL, 0.085 mmol) was added to a suspension of Cp*MoH$_3$(dppe) (54 mg, 0.085 mmol) in 1 mL of CD_3CN via microsyringe at room temperature. After 60 min, the yellow starting material had dissolved completely. Slow diffusion of Et_2O into this solution at −20 °C produced red crystals after 24 h. Yield: 15 mg (21%). A suitable crystal obtained in this manner was used for X-ray analysis. ^{1}H-NMR (CD_3CN, δ): 7.9−7.1 (m, dppe−Ph, 20H), 3.3−2.4 (m, 4H, dppe−CH_2), 2.05 (s, 6H, CH_3CN), 1.82 (s, 15H, Cp*), −4.05 (dd, 1H, MoH, $J_{HP'}$ = 10 Hz, $J_{HP''}$ = 84 Hz). Upon broad-band ^{31}P decoupling, the ^{1}H-NMR resonance at δ −4.05 collapsed into a singlet. ^{31}P-NMR (CD_3CN, δ): 52.6 (d, dppe, J_{PP} = 26.0 Hz), 76.2 (d, dppe, J_{PP} = 26.0 Hz).

Synthesis of [Cp*MoH(dppe)(MeCN)$_2$](BF$_4$)$_2$ (7). HBF$_4$·Et$_2$O (41 μL, 0.237 mmol) was added to a suspension of Cp*MoH$_3$(dppe) (101 mg, 0.160 mmol) in 2 mL of CH_3CN at room temperature, and the mixture was allowed to stir for 60 min. The solution was transferred onto a degassed chromatography column (12.6 cm × 2.3 cm) made up of acidic alumina in CH_3CN. Elution with CH_3CN yielded a yellow band, which was collected and shown by ^{1}H-NMR to contain compound **5.** The eluant was then switched to a 10:1 CH_3CN/H_2O solvent mixture, yielding a red band, which was collected. The solvent was removed under reduced pressure, and the residue was redissolved in 5 mL of fresh CH_3CN. Concentration to ca. 0.5 mL by evaporation under reduced pressure, and addition of 10 mL of Et_2O yielded the product as a red-orange precipitate. Yield: 31 mg (22%). Anal. Calcd for $C_{40}H_{46}MoP_2N_2B_2F_8$: C, 54.17; H, 5.19. Found: C, 54.29; H, 5.19. ^{1}H-NMR (CD_3CN, δ): 8.0−7.0 (m, 20H, dppe−Ph), 3.4−2.9 (m, 4H, dppe−CH_2), 2.05 (s, 3H, CH_3CN), 1.95 (s, 3H, CH_3CN), 1.63 (s, 15H, Cp*), −2.18 (dd, 1H, M−H, $J_{HP'}$ = 22 Hz, $J_{HP''}$ = 81 Hz). Upon broad-band ^{31}P decoupling, the ^{1}H-NMR resonance at δ −2.18 collapsed into a singlet. ^{31}P-NMR (CD_3CN, δ): 75.5 (d, J_{PP} = 32.6 Hz), 67.1 (d, J_{PP} = 32.6 Hz). ^{31}P{selective-^{1}H}-NMR (CD_3CN, δ): 75.5 (dd, J_{PP} = 32.6 Hz, $J_{P'H}$ = 25.0 Hz), 67.1 (dd, J_{PP} = 32.6 Hz, $J_{P''H}$ = 77.5 Hz).

Thermal Treatment of Compounds 6 and 7. Formation of Compound 8. (a) From a Mixture of 6 and 7. A solution of compounds **6** and **7** was prepared *in situ* by protonation of Cp*MoH$_3$(dppe) (59 mg, 0.094 mmol) in CD_3CN (0.5 mL), as described above. Heating this mixture to 70 °C for 105 min with ^{1}H- and ^{31}P-NMR monitoring showed an initial decrease of **7** and an increase of **6**, followed by a decrease and ultimate disappearance of **6** and formation of **8** as the only product (see Results). Compound **8**: ^{1}H-NMR (CD_3CN, δ)SPCLN 7.9−7.1 (m, dppe−Ph, 20H), 3.3−2.4 (m, 4H, dppe−CH_2), 1.85 (s, 15H, Cp*), −4.08 (dd, 1H, MoH, $J_{HP'}$ = 10 Hz, $J_{HP''}$ = 84 Hz). ^{31}P-NMR (CD_3CN, δ): 50.2 (d, J_{PP} = 25.5 Hz), 76.3 (d, J_{PP} = 25.5 Hz). The MeCN resonance is masked by the multiplet of the solvent. A saturated solution in CD_2Cl_2 shows a single MeCN resonance at δ 2.00 (6H).

(b) From Pure 6. A solution of **6** (25 mg) in CD_3CN (0.028 mL) was heated to 70 °C for 30 min. The hydride region of the ^{1}H-NMR spectrum showed the disappearance of all of the resonances due to compound **6** and the growth of the reso-

Table 1. Crystal Data for All Compounds

	1	4	6
formula	$C_{36}H_{42}MoP_2$	$C_{36}H_{43}BF_4P_2W$	$C_{40}H_{46}B_2F_8MoN_2P_2$
fw	632.58	808.30	886.29
space group	$P2_1/c$	$P2_1/n$	$Pna2_1$
a, Å	10.5920(6)	14.3353(13)	22.245(2)
b, Å	29.010(2)	16.3703(11)	10.6805(9)
c, Å	11.3044(9)	14.8550(14)	16.9237(11)
b, deg	114.402(5)	100.45(2)	
V, Å^3	3163.3(4)	3428.2(5)	4020.9(6)
Z	4	4	4
d_{calcd}, Mg/m^3	1.328	1.566	1.464
m(Mo Kα), mm^{-1}	0.539	3.509	0.475
radiation (monochromated in incident beam)		Mo Kα (λ = 0.71073 Å)	
temp, K	153(2)	153(2)	153(2)
final R indices [$I > 2\sigma(I)$]			
R1[a]	0.0545	0.0569	0.0338
wR2[b]	0.1006	0.1073	0.0735
R indices (all data)			
R1[a]	0.0763	0.0810	0.0461
wR2[b]	0.1080	0.1148	0.0798

[a] $R1 = \Sigma||F_o| - |F_c||/\Sigma|F_o|$. [b] $wR2 = [\Sigma w(|F_o| - |F_c|)^2/\Sigma w|F_o|^2]^{1/2}$; $w = 1/\sigma^2(|F_o|)$.

nances of compound **8**. No indication of the formation of **7** was evidenced.

X-ray Crystallography. (a) Compound 1. An orange parallelepiped crystal with dimensions of 0.50 × 0.225 × 0.125 mm was placed and optically centered on the Enraf-Nonius CAD-4 diffractometer. The crystal cell parameters and orientation matrix were determined from 25 reflections in the range 17.6° < θ < 20.7° and confirmed with axial photographs. Data (5852 reflections) were collected (Mo Kα) with $\omega/2\theta$ scans in the $\pm h,k,-l$ quadrant over the range 2.2 < θ < 25.0° with a scan width of (0.71 + 0.47 tan θ)° and variable scan speed of 2.0−2.3° min^{-1}, with each scan recorded in 96 steps with the outermost 16 steps on each end of the scan being used for background determination. Six standard reflections well-dispersed in reciprocal space were monitored at 1 h intervals of X-ray exposure. Minor variations in intensity were observed, and the data were not corrected for decay. An absorption correction was applied based upon crystal faces with transmission factors ranging from 0.8854 to 0.9382. Data were corrected for Lorentz and polarization factors and reduced to F_o^2 and $\sigma(F_o^2)$. Intensity statistics and systematic absences clearly determined the centrosymmetric monoclinic space group $P2_1/c$ (no 14). Averaging of equivalent reflections led to 5554 unique intensities (R(int) = 0.0288). The structure was determined by direct methods with the successful location of all non-hydrogen atoms and refined by full-matrix least-squares cycles. A subsequent difference-Fourier map revealed the location of several of the remaining hydrogen atoms within the molecule. Since many were missing, all of the hydrogen atoms bonded to carbon atoms were placed in calculated positions, with the aromatic hydrogen atoms at d_{CH} = 0.950 Å and $U_H = 1.2U_C$, the CH_2 hydrogen atoms at d_{CH} = 0.990 Å and $U_H = 1.2U_C$, and CH_3 hydrogen atoms at d_{CH} = 0.980 Å and $U_H = 1.5U_C$. The initial configuration of the CH_3 groups was determined with a rotational difference-Fourier map about the central carbon atom and was further optimized under the constraint of tetrahedral geometry. After several cycles of refinement, all of the non-hydrogen atoms were refined anisotropically and another difference-Fourier map revealed three possible locations for hydrides bound to the central Mo atom. Two of these were the highest peaks in the map (0.75 and 0.68 e Å^{-3}), while the third potential hydride was the fifth highest peak (0.45 e Å^{-3}). These three hydrides were allowed to refine freely (x, y, z, U). The structure was refined to convergence ($\Delta/\sigma \leq 0.001$), and a final difference-Fourier map was featureless with $|\Delta\rho| \leq 0.57$ e Å^{-3}. The function minimized during the full-matrix least-squares refinement was $\Sigma w(F_o^2 - F_c^2)$, where $w = 1/[\sigma^2(F_o^2) + (0.0297P)^2 + 6.5319P]$ and $P = (\max(F_o^2, 0) + 2F_c^2)/3$. An empirical correction for extinction was found to be negative and not applied. The crystal data and refinement parameters are collected in Table 1, and selected bond distances an angles are listed in Table 2.

Table 2. Selected Bond Distances (Å) and Angles (deg) for Compound 1[a]

Mo(1)−P(1)	2.3560(12)	Mo(1)−C(4)	2.321(4)
Mo(1)−P(2)	2.3797(12)	Mo(1)−C(5)	2.342(5)
Mo(1)−CNT	2.006(5)	Mo(1)−H(1)	1.65(5)
Mo(1)−C(1)	2.333(5)	Mo(1)−H(2)	1.57(5)
Mo(1)−C(2)	2.353(5)	Mo(1)−H(3)	1.55(5)
Mo(1)−C(3)	2.347(5)		

P(1)−Mo(1)−P(2)	81.21(4)	P(2)−Mo(1)−H(3)	68(2)
P(1)−Mo(1)−CNT	140.3(1)	CNT−Mo(1)−H(1)	106(2)
P(1)−Mo(1)−H(1)	60(2)	CNT−Mo(1)−H(2)	102(2)
P(1)−Mo(1)−H(2)	66(2)	CNT−Mo(1)−H(3)	114(2)
P(1)−Mo(1)−H(3)	96(2)	H(1)−Mo(1)−H(2)	123(3)
P(2)−Mo(1)−CNT	132.6(1)	H(1)−Mo(1)−H(3)	135(3)
P(2)−Mo(1)−H(1)	70(2)	H(2)−Mo(1)−H(3)	66(3)
P(2)−Mo(1)−H(2)	119(2)		

[a] CNT is the centroid of atoms C(1)−C(5).

(b) Compound 4. A colorless plate with dimensions of 0.225 × 0.175 × 0.038 mm was placed and optically centered on the Enraf-Nonius CAD-4 diffractometer. The crystal cell parameters and orientation matrix were determined from 25 reflections in the range 15.7° < θ < 17.8° and confirmed with axial photographs. Data (18 511 reflections with indices $\pm h,-k,l$ and $\pm h,\pm k,-l$) were collected as described above for compound **1**. No decay correction was necessary. An absorption correction was applied based upon crystal faces with transmission factors ranging from 0.5551 to 0.8680. Data were corrected for Lorentz and polarization factors and reduced to F_o^2 and $\sigma(F_o^2)$. Intensity statistics and systematic absences clearly determined the centrosymmetric monoclinic space group $P2_1/n$ (no 14), nonstandard setting for $P2_1/c$. Averaging of equivalent reflections led to 6006 unique intensities (R(int) = 0.1053). The structure was determined by direct methods with the successful location of the W and P atoms, along with several C atoms. Refinement by alternating full-matrix least-squares cycles and difference-Fourier maps revealed the location of the remaining non-hydrogen atoms. After several cycles of refinement, all of the non-hydrogen atoms were refined anisotropically. Hydrogen atoms attached to carbon atoms were placed in calculated positions, as described above for compound **1**. Four hydride H atoms were located from the highest peaks near the tungsten atom, with W−H distances ranging from 1.3 to 1.6 Å. These four positions are tentative at best and more speculative than definitive. They were initially refined freely, but were found to move continuously and were, therefore, subsequently restrained in their refinement in such a way that the W−H distance be near 1.6 Å and

Table 3. Selected Bond Distances (Å) and Angles (deg) for Compound 4[a]

W(1)−P(1)	2.477(2)	W(1)−C(4)	2.344(9)
W(1)−P(2)	2.508(2)	W(1)−C(5)	2.291(8)
W(1)−CNT	1.990(9)	W(1)−H(1)	1.58(5)
W(1)−C(1)	2.296(8)	W(1)−H(2)	1.57(4)
W(1)−C(2)	2.338(9)	W(1)−H(3)	1.67(4)
W(1)−C(3)	2.372(8)	W(1)−H(4)	1.65(4)
P(1)−W(1)−P(2)	78.72(7)	CNT−Mo(1)−H(1)	97(3)
P(1)−W(1)−CNT	162.8(2)	CNT−Mo(1)−H(2)	107(3)
P(1)−W(1)−H(1)	70(3)	CNT−Mo(1)−H(3)	111(2)
P(1)−W(1)−H(2)	76(3)	CNT−Mo(1)−H(4)	93(3)
P(1)−W(1)−H(3)	78(2)	H(1)−W(1)−H(2)	134(4)
P(1)−W(1)−H(4)	74(2)	H(1)−W(1)−H(3)	75(4)
P(2)−W(1)−CNT	118.4(2)	H(1)−W(1)−H(4)	80(4)
P(2)−W(1)−H(1)	127(3)	H(2)−W(1)−H(3)	128(4)
P(2)−W(1)−H(2)	74(3)	H(2)−W(1)−H(4)	60(4)
P(2)−W(1)−H(3)	57(2)	H(3)−W(1)−H(4)	147(3)
P(2)−W(1)−H(4)	131(3)		

[a] CNT is the centroid of atoms C(1)−C(5).

the four atoms define a plane and have similar U values, leading to smooth convergence ($\Delta/\sigma \leq 0.001$) with $R(F) = 8.10\%$, $R_w(F^2) = 11.48\%$, and GOF = 1.159 for all 6006 unique reflections [$R(F) = 5.69\%$ and $R_w(F^2) = 10.73\%$ for those 4677 data with $F_o > 4\sigma(F_o)$]. The H−W−H angles and the direction of the H_4 plane, however, were not restrained. Relative to the model without the four hydride H atoms, the final residuals are lower by ca. 0.1% (R1) or 0.2% (wR2). Although the final hydride locations are acceptable in both position and distance from the W atom, no reliability should be placed on them. A final difference-Fourier map possessed many peaks near the tungsten atom, within 1.2 Å, with the largest peak, $|\Delta\rho| \leq 1.29$ e Å^{-3}. The weighting scheme used was $w = 1/[\sigma^2(F_o^2) + (0.0389P)^2 + 9.0199P]$, P being defined as above. An empirical correction for extinction was attempted but found to be negative and not applied. The crystal data and refinement parameters are collected in Table 1, and selected bond distances an angles are listed in Table 3.

(c) Compound 6. A red block with dimensions of 0.325 × 0.175 × 0.125 mm was placed and optically centered on the Enraf-Nonius CAD-4 diffractometer. The crystal cell parameters and orientation matrix were determined from 25 reflections in the range 15.8° < θ < 16.2° and confirmed with axial photographs. Data (5439 reflections) were collected (Mo Kα) in the $-h,\pm k,-l$ quadrant as described for the above cases. No decay correction was applied. Six ψ-scan reflections were collected over the range 6.5° < θ < 10.9°; the absorption correction was applied with transmission factors ranging from 0.2592 to 0.2795. Data were corrected for Lorentz and polarization factors and reduced to F_o^2 and $\sigma(F_o^2)$. Intensity statistics and systematic absences clearly determined the centrosymmetric monoclinic space group $Pna2_1$ (no 33). Averaging of symmetry-equivalent reflections led to 2725 unique data (R(int) = 0.0591). Direct methods led to the successful location of Mo, two P, and several F and C atoms. Refinement by full-matrix least-squares cycles followed by difference-Fourier maps allowed the location of the remaining non-hydrogen atoms. Refinement of the Flack absolute structure parameter resulted in a value of 0.965(9). The structure was therefore inverted, and the new absolute structure parameter equaled −0.01(5). The H atom bonded to Mo was located directly from a difference-Fourier map and refined freely. All of the remaining H atoms were placed in calculated positions and handled as described above for compound **1**. The structure was refined to convergence ($\Delta/\sigma \leq 0.001$), and a final difference-Fourier map was featureless with $|\Delta\rho| \leq 0.42$ e Å^{-3}. The weighting scheme used was $w = 1/[\sigma^2(F_o^2) + (0.0302P)^2 + 1.6093P]$, P being defined as above. An empirical correction for extinction was found to be negative and not applied. The crystal data and refinement parameters are collected in Table 1, and selected bond distances an angles are listed in Table 4.

Table 4. Selected Bond Distances (Å) and Angles (deg) for Compound 6[a]

Mo(1)−P(1)	2.541(2)	Mo(1)−C(2)	2.247(6)
Mo(1)−P(2)	2.554(2)	Mo(1)−C(3)	2.270(7)
Mo(1)−N(51)	2.137(6)	Mo(1)−C(4)	2.380(6)
Mo(1)−N(61)	2.122(6)	Mo(1)−C(5)	2.418(6)
Mo−CNT	1.998(7)	Mo(1)−H(1)	1.69(6)
Mo(1)−C(1)	2.368(7)		
CNT−Mo(1)−P(1)	159.5(2)	P(1)−Mo(1)−H(1)	59(2)
CNT−Mo(1)−P(2)	121.6(2)	P(2)−Mo(1)−N(51)	84.7(2)
CNT−Mo(1)−N(51)	103.1(2)	P(2)−Mo(1)−N(61)	84.9(2)
CNT−Mo(1)−N(61)	104.8(2)	P(2)−Mo(1)−H(1)	138(2)
CNT−Mo(1)−H(1)	101(2)	N(51)−Mo(1)−N(61)	151.8(2)
P(1)−Mo(1)−P(2)	78.78(6)	N(51)−Mo(1)−H(1)	87(2)
P(1)−Mo(1)−N(51)	75.0(2)	N(61)−Mo(1)−H(1)	83(2)
P(1)−Mo(1)−N(61)	77.3(2)		

[a] CNT is the centroid of atoms C(1)−C(5).

Results

Syntheses and NMR Characterization. The compounds CpMH$_3$(dppe) (M = Mo, **1**; W, **2**) are produced by the reaction of Cp*MCl$_4$ and LiAlH$_4$ in the presence of dppe. The reaction presumably occurs via the formation of a monodentate phosphine adduct Cp*MCl$_4$(η^1-dppe), see eq 1, as indicated by the EPR resonance (doublet, $g = 1.960$, $a_P = 27.5$ G) obtained by mixing Cp*MoCl$_4$ and dppe without the aluminum reagent. The

$$\text{Cp*MCl}_4 \xrightarrow{\text{dppe}} \text{Cp*MCl}_4(\eta^1\text{-dppe}) \xrightarrow[\text{2. MeOH}]{\text{1. LiAlH}_4} \begin{matrix}\text{Cp*MH}_3\text{(dppe)} \\ \text{M = Mo, } \mathbf{1} \\ \text{W, } \mathbf{2}\end{matrix} \quad (1)$$

corresponding W derivative shows only a broad EPR resonance with no discernible P coupling. The addition of dppe to the Cp*MCl$_4$ compounds is a rapid and quantitative reaction, both in toluene and in THF. The reduction by LiAlH$_4$, on the other hand, proceeds slowly, even when the Li reagent is solubilized by the addition of ether.

It is interesting to observe that a spontaneous reduction occurs for the system in eq 1, whereas the same synthetic procedure on the related complex Cp*MoCl$_4$(PMe$_3$) produces the pentahydride product of formal oxidation, Cp*MoH$_5$(PMe$_3$).[51] Depending on the conditions, the reaction leads to contamination of the product with minor amounts of what appears to be Cp*MH$_5$(η^1-dppe) (M = Mo or W), as suggested by a doublet hydride resonance at δ −3.06 (J_{PH} = 46.2 Hz) for Mo or −2.40 (J_{PH} = 50.9 Hz) for W. The formation of this by-product can be minimized by using the toluene/Et$_2$O solvent mixture in the proportions indicated in the Experimental Section. The use of a larger proportion of Et$_2$O leads to increased amounts of the pentahydride by-product (as does the use of THF), whereas the use of neat toluene leads to unsatisfactorily slow reactions. Longer reaction times than 12 h led to the formation of increasing amounts of other uncharacterized by-products. The MeOH quenching procedure is also worth briefly discussing. The MeOH quencher improves the yield for both Mo and W systems, but also produces varying amounts of the pentahydride by-product. During the synthesis of **1**, little if any pentahydride is produced, whereas substantial amounts of this by-

(51) Shin, J. H.; Parkin, G. *Polyhedron* **1994**, *13*, 1489−1493.

product are produced during the synthesis of **2**. Therefore, the best procedure for the synthesis of **2** involves isolation of the pure trihydride before being quenched by MeOH, followed by quenching of the residue to recover additional amounts of impure **2**, which is subsequently recrystallized.

Both compounds **1** and **2** exhibit the expected NMR properties. In particular, the hydride ligands display a single resonance at δ −5.27 (**1**) or −5.90 (**2**) with coupling to two equivalent P nuclei (J_{PH} = 42.0 Hz for **1** and 44.6 Hz for **2**), indicating high fluxional behavior. The hydride resonance of the tungsten derivative also shows the expected satellites, with J_{WH} = 54.4 Hz. These properties correspond to those reported for other derivatives of the same stoichiometry.[42−46] Compounds $(C_5H_4Pr^i)MoH_3(PMe_3)_2$ and $CpMoH_3(PMe_2Ph)_2$, in particular, had been investigated at temperatures as low as −90 °C without the observation of a decoalescence of the hydride resonance.[44,46] The same behavior is observed for compounds **1** and **2**, the triplet hydride resonance remaining sharp at −90 °C.

The reaction of **1** or **2** with 1 equiv of $HBF_4 \cdot Et_2O$ in diethyl ether at room temperature precipitated $[Cp^*MH_4(dppe)]BF_4$ (M = Mo, **3**; W, **4**) in high yields, see eq 2.

$$Cp^*MH_3(dppe) + HBF_4 \rightarrow [Cp^*MH_4(dppe)]^+BF_4^- \quad \begin{matrix} M = Mo, \mathbf{3} \\ W, \mathbf{4} \end{matrix} \qquad (2)$$

Compound **3** is unstable and loses H_2 upon dissolution into any coordinative solvent (*vide infra*). Dissolution in CH_2Cl_2 at room temperature also induced H_2 loss and decomposition to unknown products. The formation of this compound is related to its immediate precipitation from the reaction medium. The crude material, which is probably already contaminated by products of H_2 loss, cannot be recrystallized, and satisfactory analytical data could, consequently, not be obtained. The NMR properties of the crude product could, however, be investigated in $CDFCl_2$ at −60 °C, under which conditions little decomposition occurs. Compound **4**, on the other hand, is stable even in MeCN at room temperature, and single crystals for an X-ray analysis (*vide infra*) could be grown from $MeCN/Et_2O$.

The ^{1}H-NMR spectra of **3** and **4** exhibit a single resonance for the four hydride ligands, which is downfield-shifted ($\Delta\delta$ = +1.71 for Mo, +3.17 for W) and more weakly coupled (ΔJ_{PH} = −6.0 Hz for Mo, −12.0 Hz for W; ΔJ_{HW} = −16.7 Hz for W) relative to **1** and **2**, respectively. The $^{31}P\{^1H\}$-NMR resonances of **3** and **4** are upfield-shifted ($\Delta\delta$ = −18.9 for Mo, −16.3 for W) relative to **1** and **2**, respectively, and the P-W coupling is reduced for **4** relative to **2** (ΔJ_{PW} = −8.9 Hz). The presence of four hydride ligands is indicated by the quintet pattern in the selectively ^{1}H-decoupled ^{31}P-NMR spectra of **3** and **4**. Cooling to −90 °C has no effect on the line shape of the ^{1}H- and ^{31}P-NMR resonances of compound **3**. On the other hand, the ^{31}P-NMR resonance of **4** has decoalesced at this temperature into two doublets at δ 48.6 and 54.7 (J_{PP} = 26.3 Hz). This indicates the inequivalence of the two P donors in the solution structure and agrees with the solid state structure (*vide infra*). This decoalescence is also reflected in the shape of the ^{1}H-NMR resonance for the hydride ligands (see Figure 1). This resonance, however, does not turn into the expected doublet of doublets for a frozen P_2 system and averaged H_4 system, thus indicating that the fast exchange of the four H ligands may also start to freeze out at this temperature.

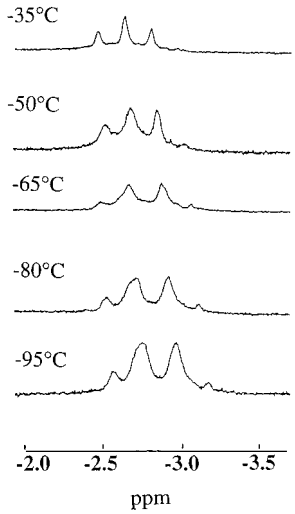

Figure 1. Variable-temperature ^{1}H-NMR spectrum of compound **4** in $CDFCl_2$.

Addition of acetonitrile to **3** at room temperature induces gas evolution and the formation of **5** as the only observed product, see eq 3. The $^{31}P\{^1H\}$-NMR spectrum

$$[Cp^*MoH_4(dppe)]^+BF_4^- + MeCN \rightarrow [Cp^*MoH_2(MeCN)(dppe)]^+BF_4^- + H_2 \quad (3)$$
$$\mathbf{5}$$

of **5** exhibits a singlet at room temperature for the coordinated dppe ligand, which splits into a triplet (J_{PH} = 52 Hz) upon selective ^{1}H decoupling, proving that the compound is a dihydride derivative. The $^{31}P\{^1H\}$ singlet is decoalesced at 193 K into two doublets at δ 82.8 and 75.3 (J_{PP} = 20.8 Hz), indicating that the two phosphorus atoms are in an inequivalent coordination environment and that the room temperature spectrum is the result of a fluxional process. The averaging of the P nuclei is also noticeable in the line shape of the hydride resonance in the ^{1}H-NMR spectrum: the single hydride resonance at −5.50 ppm is a binomial triplet (J_{PH} = 53 Hz) at high temperature (80 °C) but it broadens upon cooling. At the lowest achieved temperature (−90 °C), however, the signal has not yet achieved the slow exchange limit (see Figure 2). The line shape appears more complicated than the doublet of doublets expected for two equivalent H nuclei coupled to two inequivalent P nuclei, thus indicating that decoalescence of two inequivalent and rapidly exchanging H nuclei is also taking place.

Compound **5** is also a product of the direct protonation of **1** in MeCN. This procedure, however, also results in the formation of two isomers of a product of double protonation $[Cp^*MoH(MeCN)_2(dppe)](BF_4)_2$, **6** and **7**, both of which have been isolated. The formation of these double protonation products occurs even when a substoichiometric amount of acid is slowly added to compound **1**. Redissolution of isolated **5** in MeCN and protonation with $HBF_4 \cdot Et_2O$ also leads to the formation of **6** and **7**. Whatever the method of generation of these two compounds, their initial relative ratio is always ca. 1:3. An intermediate during the transformation of

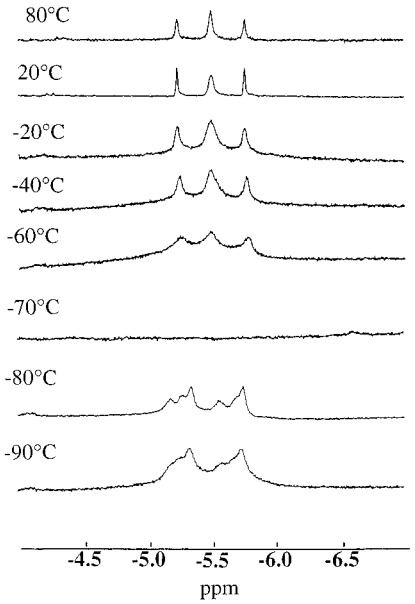

Figure 2. Temperature dependence of the ^{1}H-NMR hydride resonance of compound **5**. The solvent is CD_3CN for the spectra at 80 and 20 °C and CD_2Cl_2 for all the other spectra.

complex **5** into **6** and **7** could not be observed: protonation in CD_2Cl_2 at low temperature led to immediate loss of the hydride signal and formation of uncharacterized, hydride-free products.

Compound **6** crystallizes selectively from a solution containing compounds **5**, **6**, and **7**. Its X-ray structure has been determined (*vide infra*). The ^{1}H-NMR spectrum of **6** exhibits a doublet of doublets at room temperature for the hydride resonance at −4.05 ppm, with one small and one large phosphorus coupling. Broad-band P decoupling collapses this resonance into a singlet. The ^{31}P{^{1}H}-NMR spectrum shows two mutually coupled doublets, consistent with a rigid structure containing inequivalent phosphorus donors.

Spectroscopically and analytically pure **7** is obtained by chromatographic separation from the mixture containing **6** and **7** over acidic alumina. While **6** is trapped by the column, **7** can be eluted by a MeCN/H_2O mixture. The NMR spectroscopic properties of compound **7** are similar to those of compound **6**. The ^{1}H-NMR spectrum exhibits a doublet of doublets hydride resonance at −2.18 ppm, with one small and one large phosphorus coupling, which collapsed into a singlet by broad-band P decoupling, and two mutually coupled doublets are observed in the ^{31}P{^{1}H}-NMR spectrum. The elemental analysis is consistent with the same stoichiometry as **6**. The presence of a single hydride ligand is further confirmed by a ^{31}P{selective-^{1}H}-NMR spectrum: the two doublets split into doublets of doublets, the downfield and the upfield resonances showing HP coupling corresponding to the small and the large HP couplings, respectively, observed for the hydride resonance in the ^{1}H-NMR spectrum. An important difference between **6** and **7**, however, is the observation of two distinct MeCN resonances for **7**, whereas **6** shows a single resonance for two equivalent MeCN ligands. No discernible J_{HP} coupling is observed for the ^{1}H-NMR resonance of coordinated MeCN for any of the compounds described in this contribution, even with the use of resolution enhancement.

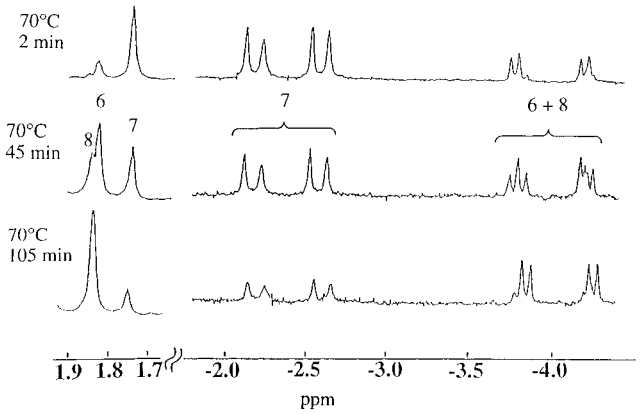

Figure 3. Representative ^{1}H-NMR spectra for the thermal treatment of a mixture of compounds **6** and **7** in CD_3CN. The different regions of the spectra are on different vertical scales.

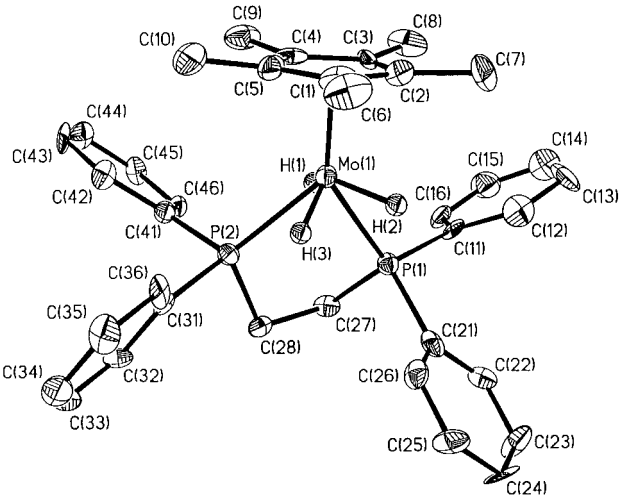

Figure 4. A ORTEP view of the molecular geometry for compound **1**. Ellipsoids are drawn at the 30% probability level.

Warming a mixture of **6** and **7** in CD_3CN to 70 °C for 2 h with ^{1}H- and ^{31}P-NMR monitoring initially shows a decrease in intensity for the resonances of **7** and a simultaneous increase for the resonances of **6**. We conclude that **6** and **7** are geometric isomers, the former being thermodynamically preferred. Obviously, the formation of a nonequilibrium ratio of **6** and **7** by protonation of **5** indicates that the two isomers must be formed by kinetically controlled independent pathways. Continued thermal treatment of the mixture of **6** and **7**, however, reveals the formation of another product, **8**, whose NMR properties are *extremely close* to those of **6**, see Figure 3. The formation of **8** is quantitative. Warming a solution of pure **6** also produces selectively and quantitatively **8**, without the detection of **7**. The cation of compound **8** appears, therefore, to be yet another isomer of [Cp*MoH(MeCN)$_2$(dppe)]$^{2+}$, whose structure must be quite close to that of **6**. Compound **8** resembles **6** also in having a single resonance for the two MeCN ligands.

Structural Characterizations. The single-crystal X-ray structure of compound **1** is shown in Figure 4. The position of the three hydrides was directly located from the difference-Fourier synthesis and refined without contraints. The coordination geometry can be related to a pseudo trigonal prism, with the center of

Chart 1

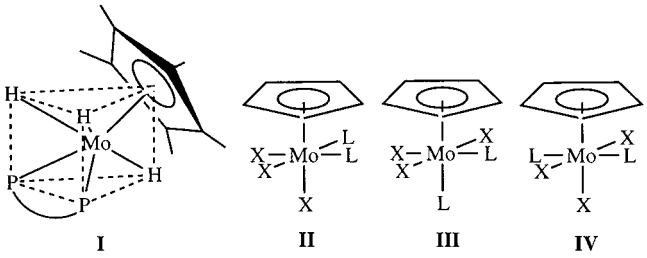

the Cp* ligand and two hydride ligands defining one triangular face and the dppe and the third hydride ligand defining the opposite triangular face, as illustrated schematically in **I**, Chart 1. The ubiquitous geometry for a (ring)MX_3L_2 stoichiometry, on the other hand, is the pseudo octahedron, for which three different stereochemistries (**II**−**IV**) are possible. Examples for each of the pseudo octahedral geometries have previously been reported, for instance $CpMoCl_3[P(OCH_2)_3CEt]_2$ of type **II**,[52] $CpMoCl_3(L-L)$ (L−L = dppe[53] or dmpe[54]) of type **III**, and $CpMoCl_3(PMe_2Ph)_2$ of type **IV**.[55] The only other previously reported solid state structure of a trihydride compound having the (ring)MH_3L_2 stoichiometry is for $CpMoH_3(PMe_2Ph)$, which is of type **IV**.[46]

For a regular trigonal prism, identical CNT−Mo−P angles should be observed. Compound **1** exhibits only slightly different CNT−Mo−P angles, indicating a small twist toward an octahedral geometry. The difference between these angles should be much greater in a structure of type **III** (e.g., see the structure of **6** below), whereas the CNT−Mo−P angles should be much smaller for a structure of type **II**. In addition, the Mo atom is displaced significantly from the plane defined by CNT and the two P atoms (by 0.283 Å), one hydride ligand being located on one side of the plane and the other two hydride ligands being located on the other side, as can be clearly seen from the top view in Figure 5.

The average Mo−P distance of 2.368(12) Å is far shorter than those in the isoelectronic $CpMoCl_3(dppe)$,[53] which is of type **III** (axial, 2.521(2) Å; equatorial, 2.688(4) Å), and $CpMoCl_3(PMe_2Ph)_2$ (average 2.554(1) Å), which is of type **IV**.[56] It is, on the other hand, similar to the average Mo−P distance in $CpMoH_3(PMe_2Ph)_2$ (2.407(3) Å), also of type **IV**.[46] If these distances are regulated mostly by steric interactions, the replacement of three Cl ligands with three H ligands is more important than the replacement of the Cp with Cp*. The less electronegative H ligands could also have the effect of expanding the metal orbitals and favoring stronger Mo−P covalent interactions (both σ and π). The Mo−H distances average 1.59(5) Å, which compares with 1.52(4) Å for $(C_5Me_4Et)MoH_5(PMe_3)$[51] and with 1.64(5) Å for $CpMoH_3(PMe_2Ph)_2$.[46] The only available Mo−H distances from neutron diffraction studies appear to be those of $Cp^*MoH(CO)_3$ (1.789(7) Å)[57] and $CpMoH(CO)_3$ (1.720(5) Å).[58] The metal−hydrogen distances determined by X-ray diffraction are usually an underestimation of the real internuclear distances, but shorter Mo−H distances relative to the above mentioned cyclopentadienyl tricarbonyl derivatives are also expected because of the higher formal oxidation state. The distance between H(2) and H(3) of 1.71 Å is much longer than the longest separation reported for a "dihydrogen" ligand, e.g., 1.357(7) Å for $ReH_7[P(p\text{-tolyl})_3]_2$;[59] thus, **1** can be considered as a classical trihydride complex. Given the similarity of the atomic radii of Mo(IV) and W(IV),[60] we assume that the structure of **2** is identical to that of **1**.

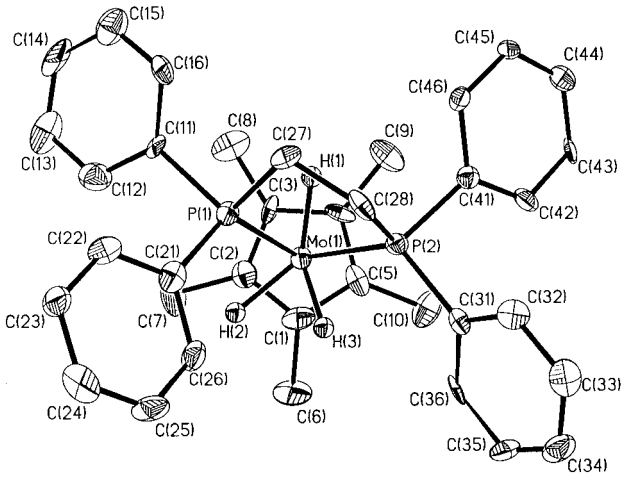

Figure 5. A top view of the compound **1**. Drawing parameters are as for Figure 4.

Compound **3** could not be structurally investigated in the solid state because the thermal instability prevents the growth of single crystals, and the solution characterization by NMR does not allow a conclusive structural assignment. The related tungsten compound **4**, on the other hand, provided suitable single crystals for an X-ray crystallographic investigation. Unfortunately, the location of the hydride ligands was not as clear cut as for the above described compound **1** (see Experimental Section). The use of restraints on the the W−H distances and the H_4 plane, but allowing free refinement of the H−W−H angles and the orientation of the H_4 plane, led to the determination of the distorted pseudo pentagonal bipyramid shown in Figure 6. The P atom is only 0.27 Å away from the least-squares H_4 plane, and the five angles between adjacent bonds in the pseudo pentagonal plane are relatively similar. The deviation of the ideal parallelism between the pseudo pentagonal plane and the Cp* ring is probably caused by the steric repulsion between the bulky equatorial PPh_2 ligand and the Cp* ring. The axial W−P bond is almost perfectly perpendicular to the least-squares pentagonal plane, while the W-CNT vector is tilted from this plane by ca. 20°. As a result, the P(1)−W−L (L = equatorial ligand) angles are essentially equivalent (average 75(4)°), whereas the CNT−W−L angle is greater for L = P(2), intermediate for L = H(2) and H(3)

(52) Poli, R.; Kelland, M. A. *J. Organometal. Chem.* **1991**, *419*, 127−136.
(53) Stärker, K.; Curtis, M. D. *Inorg. Chem.* **1985**, *24*, 3006−3010.
(54) Owens, B. E.; Poli, R. *Inorg. Chim. Acta* **1991**, *179*, 229−237.
(55) Abugideiri, F.; Gordon, J. C.; Poli, R.; Owens-Waltermire, B. E.; Rheingold, A. L. *Organometallics* **1993**, *12*, 1575−1582.
(56) Abugideiri, F.; Keogh, D. W.; Poli, R. *J. Chem. Soc., Chem. Commun.* **1994**, 2317−2318.
(57) Brammer, L.; Zhao, D.; Bullock, R. M.; McMullan, R. K. *Inorg. Chem.* **1993**, *32*, 4819−4824.
(58) Koetzle, T. F. Personal communication. See also footnote 7b in ref 57.
(59) Brammer, L.; Howard, J. A. K.; Johnson, O.; Koetzle, T. F.; Spencer, J. L.; Stringer, A. M. *J. Chem. Soc., Chem. Commun.* **1991**, 241−243.
(60) Pauling, L. *The Nature of the Chemical Bond*, 3rd ed.; Cornell University Press: Ithaca, New York, 1960.

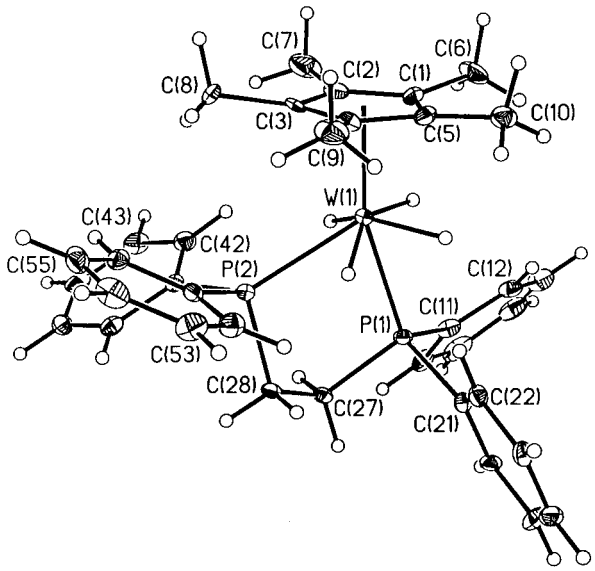

Figure 6. An ORTEP view of the molecular geometry for the cation of compound **4**. Ellipsoids are drawn at the 30% probability level.

(i.e., the hydride ligands *cis* relative to P(2)), and smaller for L = H(1) and H(4).

Even when the less accurately determined hydride positions are not considered, the relative positions of the Cp* and dppe ligands are most consistent with a pseudo pentagonal bipyramidal geometry. In particular, the W atom lies essentially on the plane identified by CNT and by the P(1) and P(2) atoms (deviation = 0.003 Å), and the observed CNT−W−P angles are quite different (162.8(2)° and 118.4(2)°). Possible alternative structures are based on a capped trigonal prism derived from the observed structure of **1** (*vide supra*). In the latter case, however, simple capping of a rectangular face by a hydride ligand would generate a structure such as **VI**, with similar CNT−W−P angles and with the W atom substantially off the plane defined by CNT and the two P atoms (Chart 2). An alternative capped pseudo trigonal prism where the two P donors occupy different positions, such as **VII**, would also lead to greater deviations from coplanarity of the W, P(1), P(2), and CNT positions. Furthermore, previously reported d^0 (ring)-ML_6 polyhydride structures are also based on the pseudo pentagonal bipyramid, i.e., $(C_5Me_4Et)MoH_5(PMe_3)$[51,61] and Cp^*ReH_6.[62] Possible alternatives of nonclassical dihydrogen complexes seem excluded by NMR (J_{HD} and T_1 measurements, *vide infra*).

The pseudo-equatorial W−P distance is significantly longer than the pseudo-axial one. Their average (2.49(2) Å) is close to the W−PMe_3 distances in $Cp^*WHCl(\eta^2$-$CH_2PMe_2)(PMe_3)$ (2.4805(8) Å)[63] and $Cp^*WH(PPh_2)_2$-(PMe_3) (2.476(1) Å).[63] The average W−H distance is 1.62(5), but the significance of this value is nulled by the restraints used during the refinement. X-ray determined terminal W−H bond lengths are 1.72(5) Å for $(\eta^1$-(P):η^5-$C_5Me_4CH_2PCy_2)WH(PMe_3)_2$ (a W(II) compound)[63] and 1.55(4) Å for $Cp^*WH(PPh_2)_2(PMe_3)$ (a W(IV) compound).[63] To the best of our knowledge, there are no reported terminal W−H distances from neutron diffraction studies. Two recently reported *bridging* W−H distances determined by neutron diffraction are 1.926(2) Å in $[PPN]_2[H_2W_2(CO)_8]$[64] and 1.897(5) Å in $[PPh_4][HW_2(CO)_{10}]$.[65]

The classical nature of all hydride ligands in compound **4** is consistent with the absence of visible HD coupling in the **4**-d_3 isotopomer, which was synthesized by protonation with HBF_4 of compound **2**-d_3. The latter compound is available by the same procedure described for compound **2** (see eq 1), except for the use of $LiAlD_4$ and quenching with CH_3OD. The hydride signal of this species is a sharp triplet at $\delta = -2.80$ (i.e., 0.07 ppm upfield relative to the hydride resonance of **4** in CD_2Cl_2). The fine structure due to coupling to the three D nuclei is not visible, even upon resolution enhancement. From the line width of the resonance, it is estimated that $J_{HD} \leq 1$ Hz. The proposed solid state pseudo-pentagonal-bipyramidal structure, **V**, agrees with the measured longitudinal relaxation time (T_1) for the hydride ^{1}H resonance in solution for both compounds **3** and **4**. The minimum value, $T_{1(min)}$, was measured as 59 ms for **3** at 203 K and 83 ms for **4** at 203 K (both at 200 MHz). Calculations[3] based on geometry **V** with a M−H distance of 1.71 Å (Mo) and 1.72 Å (W) (data adapted from the optimized geometries[66] of $CpMH_5(PH_3)$ with the same pentagonal bipyramidal geometry; the M−H distances determined by X-ray crystallography are not reliable and tend to be artificially shorter than the true internuclear distances) and a 15° bending of the H ligands away from the equatorial plane (from the average P(1)−W(1)−L angle of 75° in the structure of **4**, coinciding with the same angle in MP2 geometry optimized $CpMH_5(PH_3)$[66]) led to an estimation of T_1 of 172 ms for **3** and 178 ms for **4** at 200 MHz. The H−Cp* and H−dppe dipolar interactions were neglected in these calculations. These values are significantly larger than those determined experimentally. However, the presence of a bulky PPh_2 group in the pentagonal plane is likely to significantly distort the regular pentagon and push the hydride ligands closer to each other, reducing the calculated value of T_1. The precision of the X-ray determined hydride positions is not sufficient to verify this hypothesis. A reduction of the adjacent H···H distances from 1.94 Å to 1.62 Å for **3** and from 1.95 Å to 1.72 Å for **4** would allow a perfect fit of the data. Calculations for a pseudo octahedral nonclassical $[Cp^*MH_2(H_2)(dppe)]^+$ structure, assuming a 1.0 Å H−H distance for the dihydrogen ligand and 2.3 Å *cis* H···H contacts, lead to an estimation for T_1 of 10 ms (slow H_2 rotation limit) or 38 ms (fast rotation limit) at 200 MHz. However, stretching of the H_2 ligand to 1.0 Å and beyond usually corresponds to restrained H_2 rotation.[67] Therefore, we conclude that complexes **3** and **4** are classical tetrahydrido derivatives with a pseudo pentagonal bipyramidal structure.

The geometry of compound **6** is unambiguously determined by X-ray crystallography, including the posi-

(61) Abugideiri, F.; Kelland, M. A.; Poli, R. *Organometallics* **1993**, *12*, 2388−2389.
(62) Herrmann, W. A.; Theiler, H. G.; Kiprof, P.; Tremmel, J.; Blom, R. *J. Organometal. Chem.* **1990**, *395*, 69−84.
(63) Baker, R. T.; Calabrese, J. C.; Harlow, R. L.; Williams, I. D. *Organometallics* **1993**, *12*, 830−841.
(64) Wei, C.-Y.; Marks, M. W.; Bau, R.; Kirtley, S. W.; Bisson, D. E.; Henderson, M. E.; Koetzle, T. F. *Inorg. Chem.* **1982**, *21*, 2556−2565.
(65) Hart, D. W.; Bau, R.; Koetzle, T. F. *Organometallics* **1985**, *4*, 1590−1594.
(66) Lin, Z.; Hall, M. B. *Organometallics* **1993**, *12*, 4046−4050.
(67) Bautista, M. T.; Cappellani, E. P.; Drouin, S. D.; Morris, R. H.; Schweitzer, C. T.; Sella, A.; Zubkowski, J. *J. Am. Chem. Soc.* **1991**, *113*, 4876−4887.

Chart 2

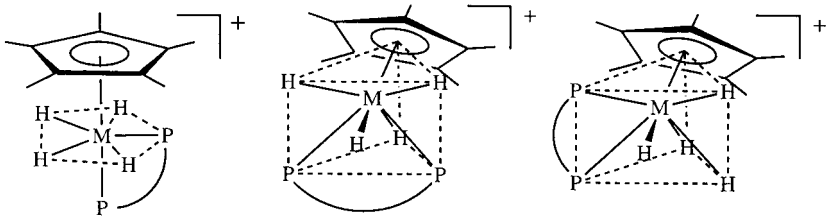

V VI VII

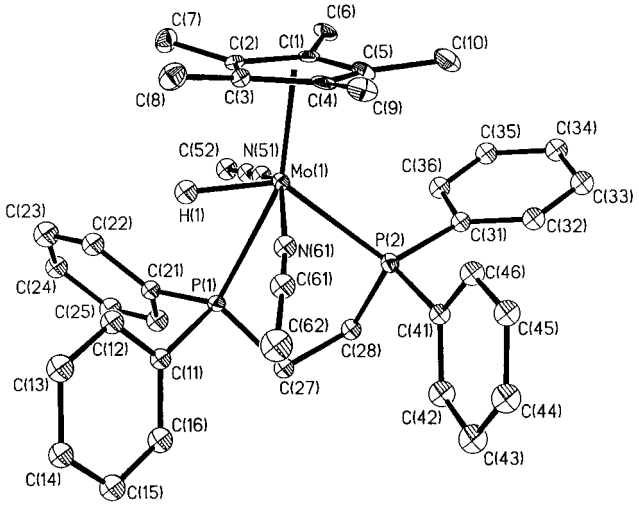

Figure 7. An ORTEP view of the molecular geometry for the cation of compound **6**. Ellipsoids are drawn at the 30% probability level.

tion of the hydride ligand which was located and freely refined. This geometry can be described as a distorted pseudo octahedron, i.e., derived from a geometry of type **III** by replacing the two relative *trans* hydride ligands with as many MeCN ligands, see Figure 7. The steric interaction between the Cp* and equatorial PPh_2 groups causes a severe distortion, which compresses the P(1) donor against the hydride ligand (P(1)−Mo−H(1) = 59(2)°). As found for the structure of **4** described above, the CNT−Mo−P angles are quite different from each other (104.8(2)° and 159.5(2)°) and the Mo atom lies essentially in the plane defined by the two P atoms and CNT (deviation 0.033 Å). The Mo−H distance of 1.69(6) Å compares relatively well with those of compound **1**, while the Mo−P distances are significantly longer than those for **1** or $CpMoH_3(PMe_2Ph)_2$,[46] see above. This effect is consistent with either or both an increase of steric bulk or/and a reduced Mo−P electronic interaction as a result of the substitution of two H^- by two MeCN ligands.

Discussion

Basicity and Protonation. Tuning the electron density on the metal center for transition metal polyhydride complexes controls, at the same time, the basicity of the complex and the choice between classical and nonclassical structures. A greater electron density favors protonation as well as the adoption of classical structures, see Scheme 1. The effect of the metal electron density on the classical/nonclassical structural issue for cyclopentadienyl derivatives has been examined theoretically by Hall *et al.*[66,68,69] Cyclopentadienyl and phosphine coligands are strong electron donors,

Scheme 1

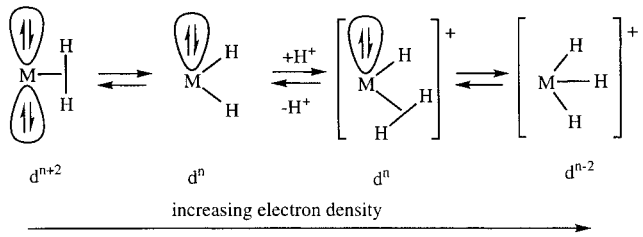

increasing the basicity at the metal center and favoring the adoption of classical structures. The above considerations rationalize rather well the observation of a classical structure for the trihydride title compounds **1** and **2** (formally d^2 complexes of Mo(IV) or W(IV)), their susceptibility to protonation, and the classical structure for their protonation products **3** and **4** (formally d^0 complexes of Mo(VI) or W(VI)).

Compounds **3** and **4** show a markedly different stability toward reductive elimination of H_2 and coordination of a donor molecule: while **3** easily loses H_2 even at low temperature in noncoordinating solvents, compound **4** is stable in MeCN at room temperature. The substitution of H_2 by MeCN in **3** to give **5** presumably takes place via the dihydrogen complex intermediate $[Cp^*MH_2(H_2)(dppe)]^+$; thus, we can imagine that the equilibrium on the right hand side of Scheme 1 is shifted further to the right for W relative to Mo, in line with the known greater basicity of 5d metals relative to their 4d counterparts.[70]

The high basicity of the systems examined in this contribution is highlighted by the occurrence of a second protonation process, followed by further H_2 loss and MeCN coordination, to form different isomers of $[Cp^*MoH(MeCN)_2(dppe)]^{2+}$. The overall process is likely to take place according to the mechanism outlined in Scheme 2. The presence of an intermediate of type **XV** or **XVI**, e.g., $[Cp^*MoH_3(MeCN)(dppe)]^{2+}$, however, could not be verified. Evidently, compound $[Cp^*MoH(\eta^2\text{-}H_2)(MeCN)(dppe)]^{2+}$ must be quite electron poor and immediately releases H_2. Other transition metal polyhydride systems that have been reported to undergo a double protonation process are $ReH_5(PPh_3)_2(py)$, $OsH_6(PPr^i_3)_2$, and $OsH_2(dppe)_2$, generating $[ReH(MeCN)_3(PPh_3)(py)]^{2+}$,[71] $[OsH_4\text{-}2n(PPr^i_3)_2(MeCN)_{2+n}]^{2+}$ (n = 0, 1),[72] and $[Os(H_2)(dppe)_2(MeCN)]^{2+}$,[73,74] respectively.

(68) Lin, Z.; Hall, M. B. *Organometallics* **1992**, *11*, 3801−3804.
(69) Bayse, C. A.; Couty, M.; Hall, M. B. *J. Am. Chem. Soc.* **1996**, *118*, 8916−8919.
(70) Collman, J. P.; Hegedus, L. S.; Norton, J. R.; Finke, R. G. *Principles and Applications of Organotransition Metal Chemistry*; University Science Books: Mill Valley, CA, 1987.
(71) Allison, J. D.; Walton, R. A. *J. Chem. Soc., Chem. Commun.* **1983**, 401−403.
(72) Smith, K.-T.; Tilset, M.; Kuhlman, R.; Caulton, K. G. *J. Am. Chem. Soc.* **1995**, *117*, 9473−9480.

Scheme 2

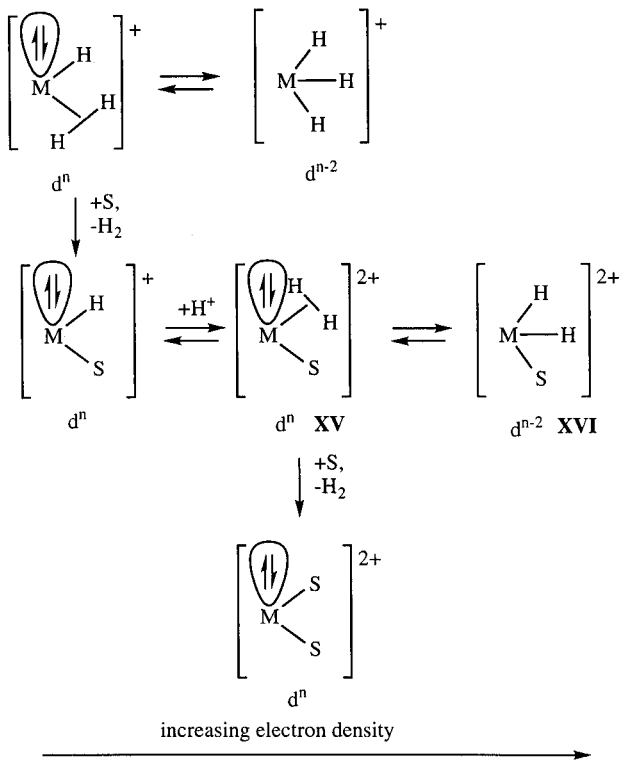

Structural Preferences. As mentioned in the Results section, the ubiquitous geometry adopted by (ring)-ML_5 complexes is the pseudo octahedron. To the best of our knowledge, there are no previous examples of (ring)ML_5 compounds with a geometry based on the pseudo trigonal prism. For a d^2 system, the pseudo-octahedral geometry should be electronically favored because the six σ bonds formed by the s, p, and d (e_g set) orbitals are augmented by the two Mo−Cp π bonds that use the d_{xz},d_{yz} set, while the two metal electrons would reside in the d_{xy} orbitals, which can engage in Mo−Cp δ back-bonding. Calculations at the MP2 level on the model system $CpMoH_3(PH_3)_2$ have shown that a pseudo-trigonal-prismatic structure like **I** is 8.95 kcal/mol higher in energy relative to the most favored structure **II**, while calculations on the sterically more hindered $CpMoH_3(PMe_3)_2$ place structure **IV** as the most stable one by 2.92 kcal relative to **II**.[46] When the two neutral L donors are connected via a backbone, such as for the dppe ligand, only type **II** and **III** structures within the pseudo-octahedral geometry could be adopted in principle. Indeed, a geometry that can be described as distorted type **III** is adopted by compound **6**. The steric interaction between the bulky dppe and Cp* ligands, however, certainly disfavors geometry **III** relative to **I**. It is quite possible that the small size of the three H^- ligands in compounds **1** and **2** can be most easily accommodated in structure **I**, whereas the exchange of two H^- with as many MeCN ligands in compound **6** introduces additional repulsive interactions (i.e., MeCN−Cp* and MeCN−dppe) that tilt the energy balance back toward geometry **III**.

Compound **5** presents an interesting case because it is sterically and electronically midway between the crystallographically characterized compounds **1** (trigonal prism) and **6** (octahedron). The NMR properties indicate fluxional sets of hydride ligands and P donors. The pseudo-octahedral structure **VIII**, therefore, is excluded because it has equivalent hydrides, Chart 3. Possible alternatives are the isomeric octahedral structure **IX** and the pseudo-trigonal-prismatic structure **X**. As dicussed more extensively below, structure **X** fits with the structural trends of the other compounds described in this paper, and an easy rationalization of the coalescence of the P and H resonances is possible. Structures **IX** and **X** allow an easy rationalization of the protonation results (formation of the two isomers **6** and **7**, see below).

As shown by Figure 3, three isomers for complex $[Cp^*MoH(MeCN)_2(dppe)]^{2+}$ have been observed by NMR. Isomer **6** has been characterized by X-ray crystallography as the pseudo-octahedral *mer,trans* isomer (see Figure 7). Several structural possibilities remain for isomers **7** and **8**. However, the inequivalence of the P donors, as shown by ^{31}P-NMR spectroscopy, excludes the possibility of symmetrical structures. A few remaining possibilities are **XI**−**XV**, Chart 4. Geometries **XI** and **XII** are based on the pseudo octahedron, while geometries **XIII**−**XV** are based on the pseudo trigonal prism. In **XIII**, both P donors are as far as possible from the Cp* ligand, as found for the structure of compound **1** (which presumably minimizes the steric repulsion between Cp* and dppe ligands), whereas in **XIV**, one P donor occupies a position adjacent to Cp*, and both P donors are adjacent to Cp* in **XV**. Additional possibilities are generated by exchanging the H and MeCN positions in **XIV**.

The pattern of J_{PH} for compounds **7** and **8** is similar to that of **6** (one small and one large J_{HP} constant), the spectrum of **8** being remarkably close to that of **6**. The observation of equivalent MeCN ligands for **8** rules out all the alternative structures **XI**−**XV** and leaves only the possibility of a geometry identical with that of **6**. The difference between **6** and **8** must therefore be due to a conformational change in the coordination periphery (i.e., the Cp* or dppe ligand). The interesting conclusion from the thermal study (see Figure 3) is that the protonation process leads selectively to the higher energy conformer (**6**), which then converts quantitatively to the more stable one (**8**).

The observation of two distinct MeCN resonances for compound **7** does not provide any additional decisive factor for the structural assignment. Additional considerations, however, can be made. As mentioned above, the pseudo octahedral geometry has an electronic preference over the pseudo-trigonal-prismatic one, whereas the pseudo-trigonal-prismatic structure is probably sterically driven by placing the two encumbered phosphorus donors further away from the Cp* ligand. It is, therefore, reasonable to assume that any other trigonal-prismatic geometry will not be favored unless both P donors are as far as possible from the Cp* ligand. This argument eliminates geometries **XIV** and **XV** from consideration. Among the pseudo-octahedral alternatives, **XII** has both P donors in a *cis* position relative to the Cp* ligand and is, thus, likely to be less stable than **XI**. Structure **XI** is similar to the structure observed for isomer **6**, except that the positions of the hydride ligand and one of the MeCN ligands are

(73) Earl, K. A.; Jia, G.; Maltby, P. A.; Morris, R. H. *J. Am. Chem. Soc.* **1991**, *113*, 3027−3039.
(74) Schlaf, M.; Lough, A. J.; Maltby, P. A.; Morris, R. H. *Organometallics* **1996**, *15*, 2270−2278.

Chart 3

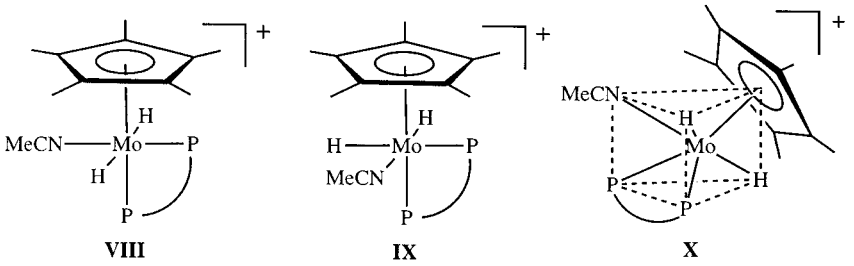

VIII **IX** **X**

Chart 4

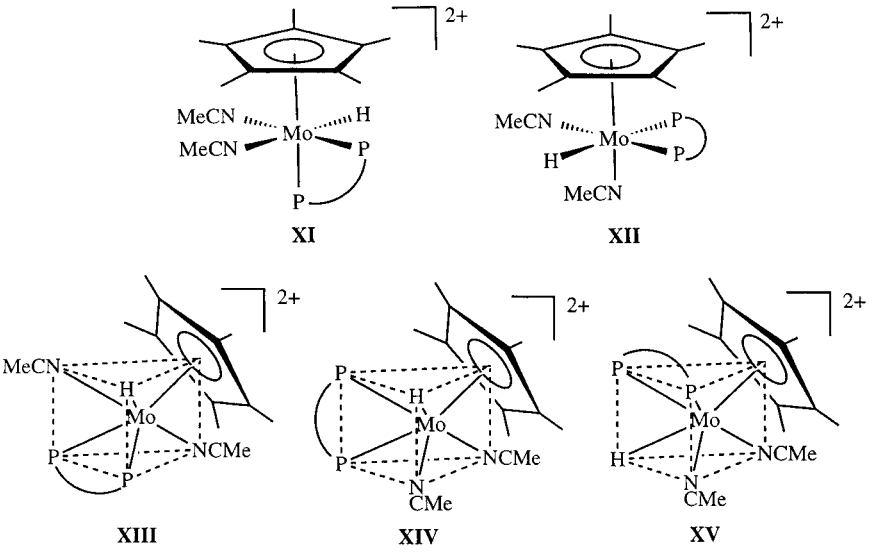

XI **XII**

XIII **XIV** **XV**

exchanged. Since the steric interaction between Cp* and dppe pushes the axial P donor close to the ligand which is located *trans* relative to the equatorial P donor (the hydride for **6**, a MeCN ligand for **XI**), structure **XI** is probably sterically less favored than **6** because of the greater bulk of MeCN relative to H. This idea would seem consistent with the lower thermodynamic stability of **7** relative to **6**. Structure **XI**, however, is not consistent with the NMR properties observed for **7**, in particular the pattern of J_{HP} values. In structure **XI**, the hydride ligand is located in a *cis* position relative to both P nuclei, leading to the expectation of similar J_{PH} values, whereas the two observed values are quite different from each other. By exclusion, we are left with **XIII** as the most likely structure for compound **7**. This structure fits the observed J_{PH} pattern, one P donor being at a much smaller angle than the other relative to the Mo−H bond. As will be seen in a later section, this assignment also allows a straightforward rationalization of the mechanistic details of the protonation and isomerization processes. Our efforts at growing single crystals of compounds **7** and **8** have not so far met with success.

One more point of structural discussion about compound **5** is proper at this point. It was previously shown that possible structures are those illustrated in **IX** and **X**. However, it has now been shown that one isomer of complex $[Cp^*MoH(MeCN)_2(dppe)]^{2+}$ (i.e., the cation of **7**) probably adopts a pseudo-trigonal-prismatic structure. For this reason, we think it more likely that **5** also adopts the pseudo-trigonal-prismatic structure **X**. If this is true, the series of compounds $[Cp^*MoH_{3-n}(MeCN)_n(dppe)]^{n+}$ show a monotonous trend of fluxionality for the same pseudo-trigonal-prismatic structure: highly fluxional for **1** ($n = 0$), fluxional at room temperature but frozen (on the ^{31}P-NMR time scale) at −80 °C for **5** ($n = 1$), and frozen at room temperature for **7** ($n = 2$).

Fluxional Mechanisms. The observation of different structures for isoelectronic compounds of the same class (i.e., pseudo trigonal prismatic for **1**, **5**, and **7**; pseudo octahedral for **6** and **8**), naturally induces us to propose an interconversion between these two structural types as the hydrogen scrambling mechanism in the various compounds. For compounds **1** and **2**, this process would indeed easily scramble all hydride ligands among all possible positions, as shown in Scheme 3. The process involves subsequent interconversions of geometries of types **I** and **III** and consists in subsequent 60° rotations of triangular faces that can be related to the Bailar twist of the true octahedral coordination geometry. This mechanism has also been recently proposed for the hydride scrambling in the isoelectronic $CpOsH_5$ compound as a result of a theoretical study.[69]

The same mechanism proposed for the hydride scrambling in compounds **1** and **2** can account for the hydride and phosphorus exchange process in **5**, see Scheme 4. It is likely that the two P and the two hydridic H nuclei in structure **XVIII** are averaged via the pseudo-octahedral structure **XIX** and the symmetric pseudo-trigonal-prismatic structure **XX**. The rearrangement via the intermediates **XXI** and **XXII** would only average the hydride resonances and not the phosphorus resonances (i.e., H_a and H_b exchange their positions, but P_b always remain the closest donor to the MeCN ligand and is thereby not exchanged with P_a). The latter process, at any rate, should be less favored than that via **XIX** and **XX**, because structure **XXI** is more steri-

Scheme 3

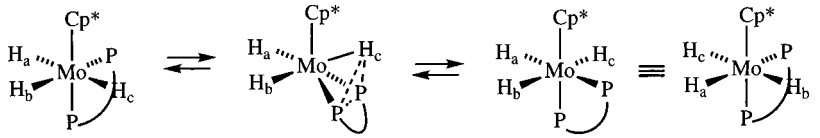

Scheme 4

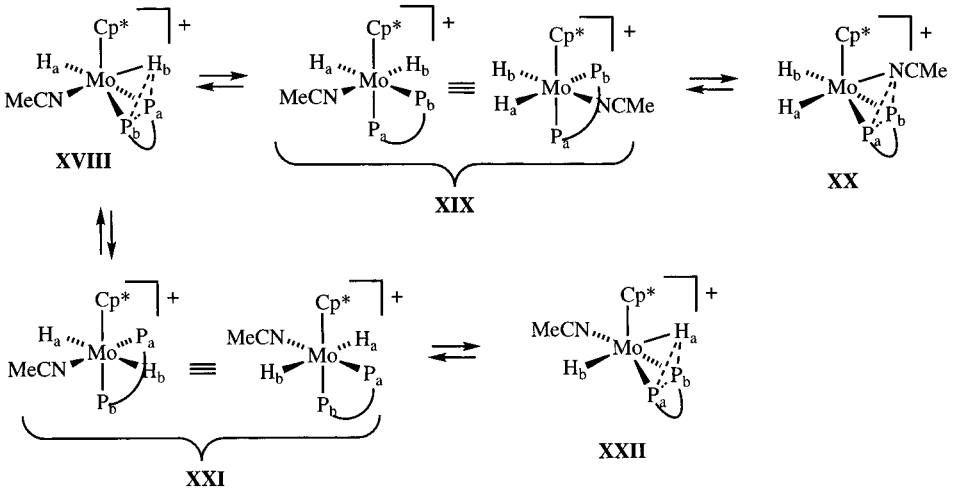

cally crowded than **XIX**, having the bulkier MeCN ligand in the crowded plane defined by the Cp* center and the dppe ligand, in close proximity to the axial P donor. The P_b−Mo−NCMe angle in **XXI** should be significantly smaller than 90° because of the distortion caused by the Cp*−dppe steric repulsion (e.g., compare with the structure of **6**). This fluxional mechanism would also be consistent with **XIX** as the ground state structure for compound **5**.

For the pseudo-pentagonal-bipyramidal compounds **3** and **4**, possible scrambling mechanisms would involve interconversion with a capped pseudo trigonal prism or with a capped pseudo octahedron. The interconversion via equilibration with a nonclassical H_2 complex and H_2 rotation, however, cannot be excluded, especially for the Mo compound.

Mechanism of Protonation of [Cp*MoH$_2$(MeCN)(dppe)]$^+$ and Isomerization of [Cp*MoH(MeCN)$_2$(dppe)]$^{2+}$. The protonation mechanism of **5** must lead independently to the different [Cp*MoH(MeCN)$_2$(dppe)]$^{2+}$ cations of **6** and **7**, since these are simultaneously produced and they do not easily interconvert. A simple scheme, which incorporates the pseudo trigonal prism−octahedron interconversion shown above in Schemes 3 and 4, leads to a satisfactory rationalization of all the observations (see Scheme 5). We propose that protonation of **5** occurs independently at the two inequivalent hydride positions H_a and H_b of structure **XVIII** (paths a and b). The protonated product, rather than collapsing to a classical trihydride derivative, loses H_2 to yield intermediates **XXIII** and **XXIV**. At this point, these intermediates can be trapped by MeCN or rearrange to a pseudo-octahedral environment, followed by MeCN trapping. Trapping of **XXIII** would produce a symmetrical pseudo-trigonal-prismatic product **XXV**, which is not observed. If this path is followed, intermediate **XXV** must have a low barrier pathway for interconversion to one of the observed isomers, e.g., **7** (see Scheme 5). Rearrangement of **XXIII**, on the other hand, leads to two different intermediates **XXVI** and **XXVII**, depending on which direction the dppe ligand swings, see Scheme 5. Intermediate **XXVI** is likely to be favored because the most sterically hindered position (meridional with the dppe ligand) is vacant, whereas this is occupied by a MeCN ligand in **XXVII**. However, both intermediates yield the same product, *cis*-[Cp*MoH(MeCN)$_2$(dppe)]$^{2+}$ (i.e., **XI**), by MeCN trapping. This is again an unobserved structure, probably because of unfavorable PPh$_2$(equatorial)−Cp* and PPh$_2$(axial)−MeCN steric interactions. These repulsions can be minimized by transformation to **7**, which requires only minimal rearrangements (a pseudo Bailar twist of the triangular face defined by the two P and one of the two MeCN donors) and is thus likely to be a fast process. Protonation of the position H_a in compound **5** according to the mechanism of Scheme 5, therefore, would lead to compound **7** as the only product. Direct trapping of intermediate **XXIV** by MeCN would lead directly to the observed pseudo-trigonal-prismatic **7**. On the other hand, rearrangement leads to intermediates **XXVIII** and **XXIX**, depending on the direction of the dppe ligand swing. The latter intermediate should be more favored than the former, because the position meridional with dppe is occupied by the less bulky hydride ligand. Trapping of **XXVIII** leads again to **XI** (which then transforms to **7**), whereas trapping of **XXIX** leads to *trans*-[Cp*MoH(MeCN)$_2$(dppe)]$^{2+}$, i.e., the cation of **6**.

Thus, this scheme rationalizes quite well the formation of both isomers **6** and **7**, the latter one being the predominant product. The exact ratio between **6** and **7** is expected to depend on several factors, such as the relative susceptibility of H_a and H_b to protonation, the relative ratio of direct MeCN trapping of **XXIII** and **XXIV** vs rearrangement, and the kinetic control of the rearrangement of **XXIV** to **XXVIII** and **XXIX**. Within this mechanistic hypothesis, the direct formation of **6** would demonstrate that at least a certain amount of intermediate **XXIV** must rearrange before being trapped by MeCN. According to the proposed scheme and structural assignments, the conversion of **7** into **6**

Scheme 5

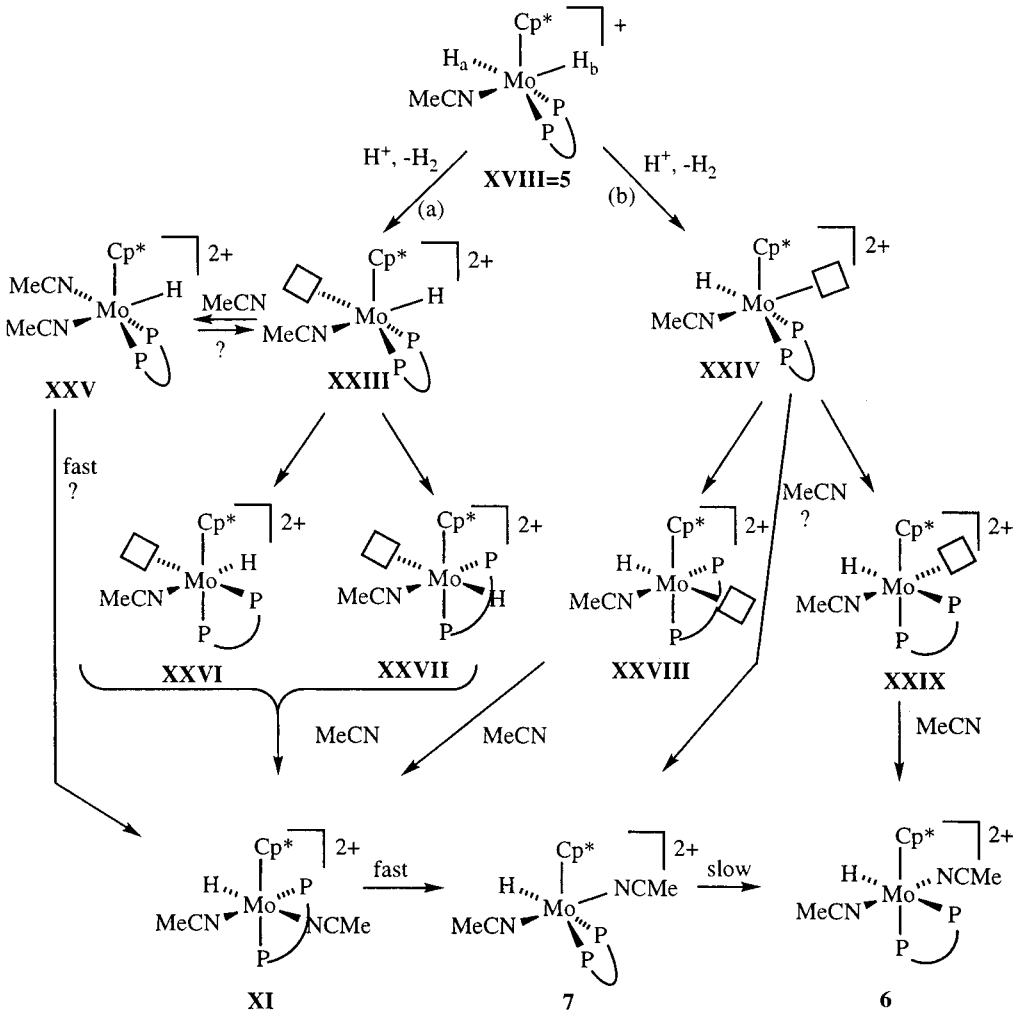

involves a further 60° pseudo Bailar twist of the same triangular face, which leads to the transformation of **XI** into the cation of **7**. Experimentally, the former process is found to be much slower than the latter, for reasons that do not appear obvious. If the cation of **5** adopted structure **XIX** as the ground state structure, the observation of a mixture of **6** and **7** under kinetically controlled conditions would still be possible: protonation of positions a and b followed by H_2 loss would lead directly to intermediates **XXVI** and **XXIX**, respectively, which would lead to the two observed products. If this were the case, however, the observed relative amounts of **6** and **7** could only be explained by a 3:1 kinetic preference for protonation of position a relative to b.

Conclusion

The compounds $Cp^*MH_3(dppe)$ (M = Mo, W) are electron-rich systems, easily yielding classical tetrahydride cationic products $[Cp^*MH_4(dppe)]^+$, which differ in stability (Mo < W) in accord with the expected greater electron donating capability of W relative to Mo. Loss of H_2 and coordination of MeCN for the Mo system triggers a second protonation process to produce two isomers of $[Cp^*MoH(MeCN)_2(dppe)]^{2+}$ under kinetically controlled conditions, while a third and thermodynamically more stable isomer is accessible thermally. This work has highlighted for the first time the involvement of pseudo-trigonal-prismatic structures for the (ring)-MH_3L_2 class of derivatives. While the observation of this structure in the ground state is probably fortuitous and related to the Cp*−dppe steric repulsion and the presence of the ethylene backbone in the dppe ligand, the occurrence of pseudo-trigonal-prismatic structures as intermediates for the hydride scrambling process in other (ring)MH_3L_2 systems may be a general phenomenon. The stepwise substitution of H^- with a MeCN ligand in the series of complexes $[Cp^*MoH_{3-n}(MeCN)_n(dppe)]^{n+}$ (n = 0, 1, 2) slows down the hydride and phosphine scrambling processes, while at the same time disfavoring the pseudo-trigonal-prismatic structure in favor of the ubiquitous pseudo-octahedral structure. It is our intent to explore next the chemical and electrochemical oxidation of compounds **1** and **2** in various solvents and the reactivity of the resulting oxidation products.

Acknowledgment. Support for this work by the Department of Energy (grant No. DEFG059ER14230 to R.P.) is gratefully acknowledged. We also thank Mr. Jung-Soo Yi for technical assistance.

Supporting Information Available: Tables of crystal data, atomic coordinates, bond distances and angles, and anisotropic displacement parameters for compounds **1**, **4**, and **6** (51 pages). Ordering information is given on any current masthead page.

OM961002O